



Electrochemical Deposition and Spectroscopy Investigation of Zn Coatings on Steel

A. El Fazazi¹ · M. Ouakki¹ · M. Cherkaoui^{1,2}

Received: 24 June 2020 / Revised: 25 September 2020 / Accepted: 21 January 2021 / Published online: 27 February 2021
© The Author(s), under exclusive licence to Springer Nature Switzerland AG part of Springer Nature 2021

Abstract

A three-electrode electrochemical cell was used for the optimization of bath constituents and parameters. Galvanostatic electrodeposition from a free additives bath, combining sulfate and chloride compounds results in bright Zn deposits with high corrosion resistance. Surface morphology was observed by scanning electron microscopy, chemical and phase composition were determined by X-ray diffraction, and corrosion investigations by electrochemical techniques. Electrochemical impedance spectroscopy (EIS) and polarization measurements revealed that the electrodeposited Zn coating with the higher current density and pH value had the best corrosion resistance. Bright and uniform surface appearance, of Zn deposits, with a platelet structure, moderate current efficiency and a high corrosion resistance was obtained at a pH of 4.5 and a current density of 16 mA cm^{-2} .

Keywords Zn electrodeposition · Corrosion · EIS · Tafel polarization · Current density · pH

1 Introduction

Zn coatings are widely used for steel protection against corrosion in many fields; electrochemical energy converters, automobile industry, aeronautic industry, batteries applications, food industry [1–6]. Zn coatings are extensively used not only because Zn is anodic to steel and thus act as a barrier on the steel surface and sacrificially protect the substrate but also owing to its low cost and natural abundance [5, 7]. The metal can be applied by a variety of techniques including hot dipping, metal spraying, cementation, cladding and electrodeposition [8]. Among them, electrodeposition offer a unique combination of superior properties such as high efficiency, corrosion resistance and low cost [5, 9, 10].

Many producers and investigators assume that the service life of the electrodeposited layers is directly proportional to

their thickness only. However, the corrosion characteristics are strongly determined by the texture and microstructure obtained that, in turn, depend on the electrochemical deposition parameters employed [11], such as current density, temperature, pH, substrate surface preparation and bath composition [12].

The absorption of hydrogen in metals is a serious problem during zinc electroplating, leading to hydrogen embrittlement of the substrate and modifications of the mechanical properties of the material and, sometimes, stress corrosion cracking. Zinc plating is in most cases carried out on steel which is one of the metals that suffers hydrogen embrittlement, and it is often said that a zinc layer acts as a barrier against hydrogen absorption. Since the overpotential for hydrogen evolution is smaller on steel than on zinc, a first hypothesis was the absorption of hydrogen by the bare steel before formation of the first zinc crystallites. A second hypothesis was the trapping of hydrogen in the deposit during zinc plating and subsequent diffusion of hydrogen in steel [13–15].

Gomes et al. [16] had realized a pulsed electrodeposition of Zinc in acidic sulphate solutions. The morphological and structural analysis showed that the Zn deposition is accompanied by the evolution and adsorption of hydrogen bubbles and in consequence the surface was not uniform.

✉ A. El Fazazi
asmae.elfazazi@uit.ac.ma

✉ M. Ouakki
moussassaw@gmail.com

¹ Laboratory of Materials, Electrochemistry and Environment (LMEE), Faculty of Sciences, University Ibn Tofail, BP 133, 14 000 Kenitra, Morocco

² National Higher School of Chemistry (NHSC), Ibn Tofail University, B.P 133, Kenitra, Morocco

Prestat et al. [17] had studied the cathodic polarization of Zinc in NaCl 6.0 M solutions. Corrosion products of mainly simonkolleite and ZnO were found to form on the surface of the electrode. This effect is assigned to the strong alkalisation of the surface due to oxygen reduction.

Many studies have been interested by the effects of electrolysis parameters, such as pH value and current density, on the crystallographic texture and surface morphology of zinc deposits on a steel substrate [11, 12, 18]. Besides, calculations and experimental determinations of some electrochemical parameters for Zn/Zn(II) on different electrodes are presented [2, 3, 8, 9, 12, 16, 19–21].

The aim of this study is to investigate the effect of current density and pH on the electrodeposition behavior, morphology as well as the corrosion resistance of Zn deposited coatings from a free additives bath. Selection of optimal operating conditions, including current density and pH, which provide the best corrosion resistance and surface appearance of the formed deposit, have also been studied. Electrochemical methods such as cyclic voltammetry (CV) and galvanostatic measurements were used to study the electrodeposition process. SEM and Energy Dispersive X-Ray (EDX) were used to characterize the morphology and the composition of the coatings. Finally, potentiodynamic polarization measurements and EIS have been carried out for the corrosion study in 3.5% NaCl.

2 Materials and Methods

2.1 Preparation of Substrates

Plates of E24 steel with a nominal chemical composition of Fe, 0.17 C, 0.045 P, 0.045 S and 0.008 N were used as the substrate. The exposed surface of steel substrates is of 1 cm². For the electrodeposited Zn coating, the substrates were abraded with different grades of emery papers from 40 to 2000 grit. These samples were degreased in acetone at room temperature, rinsed with distilled water and immediately transferred to the electroplating bath.

2.2 Coating Processes

Zn coatings were produced by direct current electrodeposition from free additives electrolytes. The bath composition and plating conditions are presented in Table 1. Analytical grade chemicals and distilled water were used for preparation of the electrolyte. The pH was adjusted by adding 1 M HCl or 1 M NaOH solutions and varied from 1.4 to 5.5. A current density in the range of -16 to -40 mA cm⁻² was applied and the temperature was set at ambient temperature 20 ± 1 °C.

Table 1 Baths composition

Electrolytes	ZnSO ₄ ·7H ₂ O (g l ⁻¹)	H ₃ BO ₃ (g l ⁻¹)	KCl (g l ⁻¹)
1	–	–	93.2
2	–	24.8	93.2
3	64.6	24.8	93.2

2.3 Corrosion Tests

Characterization of corrosion behavior of the coatings was done by three different techniques namely:

1. Measurement of the OCP (Open Circuit Potentials).
2. Potentiodynamic polarization method—measurement of corrosion potential (E_{corr}) and corrosion current (i_{corr}).
3. Determination of polarization resistance of the coatings with EIS.

The open circuit potentials (OCPs) of the coatings were measured using a PGZ 100 potentiostat in a conventional three-electrode electrochemical cell, composed of an Ag/AgCl/KCl saturated reference electrode, a platinum counter-electrode and a working electrode, namely the studied sample. The OCPs were monitored for 15 min and subsequently the electrodes were polarized potentiodynamically in a continuous sweep. The rate of potential sweep was 1 mV s⁻¹. The E_{corr} and I_{corr} were determined from the intercepts by Tafel's extrapolation method.

EIS was also performed in a three-electrode electrochemical cell as mentioned above. The electrode potential was allowed to stabilize for 15 min before starting the measurement. The EIS spectra for the coatings were acquired at OCP with AC frequencies ranging from 100 kHz to 10 mHz and amplitude of 10 mV. The obtained data of real and imaginary components were analyzed using EC-Lab and an equivalent circuit (EC) model was proposed to interpret the electrochemical impedance data.

For all the electrochemical characterization 3.5% NaCl solution was utilized which simulates the marine environment.

2.4 Characterization of Coatings

The electrodeposited surface morphologies of the coated samples, along with the chemical composition were examined using a Scanning Electron Microscopy (Quanta FEG 450) coupled with Energy Dispersive X-Ray (EDX) spectrometer and fulfilled in UATRS-CNRST-Rabat.

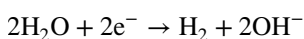
3 Results and Discussion

3.1 Effect of Current Density on Zn Deposition

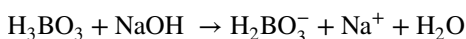
3.1.1 Voltammetric Study

Many electrolytes were used to well understand Zn deposition (Table 1). The pH was set to 4.5 with ambient temperature of 20 °C and a scan rate of 25 mV s⁻¹.

Figure 1 shows the voltammogram realized in electrolyte 1. We note that the current density is fully stable between -0.3 and -1.3 V vs. Ag/AgCl. No current was observed until the potential reaches values higher than -1.3 V, then, the cathodic current begins to increase rapidly, which is associated to hydrogen reduction according to [22]:

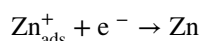
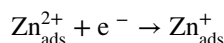
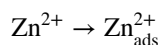


The voltammogram realized in solution containing KCl + H₃BO₃ (Fig. 2) has the same shape as in electrolyte 1. In fact, boric acid is considered a very weak acid, with a tabulated ionization constant around pK_a=9.2 [23]. Yet, in the presence of a strong base like NaOH (pK_a=14.8), a reaction takes place according to the following equation:



Therefore, boric acid doesn't have any effect on hydrogen evolution reaction.

In Fig. 3, the cathodic current increases sharply at -1.05 V vs. Ag/AgCl and gives rise to a cathodic peak at around -1.17 V vs. Ag/AgCl. This peak is related to Zn²⁺ reduction during the cathodic scan according to the following reactions [24]:



According to Zn voltammogram, the applied current densities should be superior to the limiting current density of Zn deposition, which is ≈ -10 mA cm⁻². Consequently, galvanostatic experiments were carried out in a range of current density varying from -16 to -40 mA cm⁻².

3.1.2 Gravimetric study

Figure 4 presents the variation of the deposition potential (E_d) during Zn electrodeposition with different current densities in electrolyte 3 (Table 1). A further increase in current density leads to a notable shift of E_d towards more negative values. For instance, Zn deposition at -16, -24, -32 and -40 mA cm⁻² exhibit an average deposition potential E_d of -1.42, -1.51, -1.62 and -1.85 V, respectively. A

Fig. 1 Cyclic voltammogram on a Fe substrate in KCl solution at pH 4.5 (electrolyte 1), scan rate = 25 mV s⁻¹

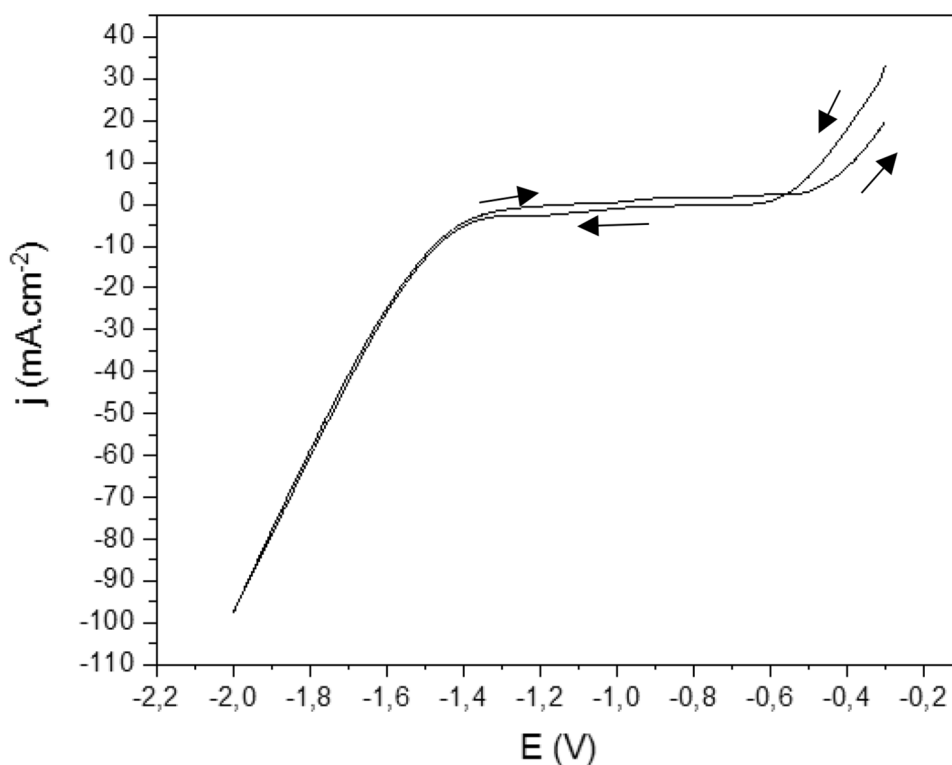
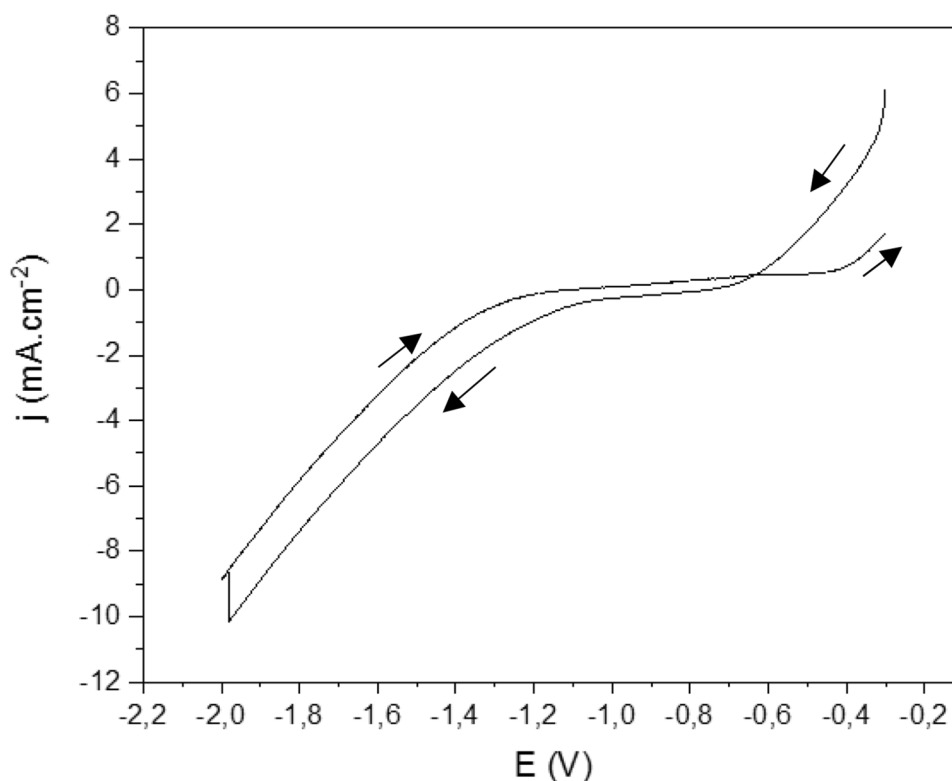


Fig. 2 Cyclic voltammogram of a Fe substrate in KCl + H₃BO₃ solution at pH 4.5 (electrolyte 2), scan rate = 25 mV s⁻¹



supplementary rise of the current density causes stronger potential oscillations in the curves due to intensive hydrogen evolution [15, 25].

The effect of current density on the thickness (e), which is given by the following relation [26]:

$$e = \Delta m / \rho S$$

where Δm (g): the deposited mass of coating; ρ (g cm⁻³): the density of coating and S (cm²): the surface area of the substrate, is shown in Table 2. It can be seen that the thickness increases with increasing current density, as well as the deposition rate v ($\mu\text{m h}^{-1}$), which is calculated according to the following equation:

$$v = (m_2 - m_1) / \rho S t$$

where m_2 (g): mass of the sample after the deposition, m_1 (g): mass of the sample before the deposition and t (s): deposition time.

Moreover, it is observed (Table 2) that the current efficiency (CE) decreases with increasing current density, which can be attributed to the rapid increase in hydrogen evolution. The CE is obtained using the equation:

$$CE = \Delta m / m_{th} * 100$$

m_{th} is calculated by the mean of Faraday's law:

$$m_{th} = jtM / nF$$

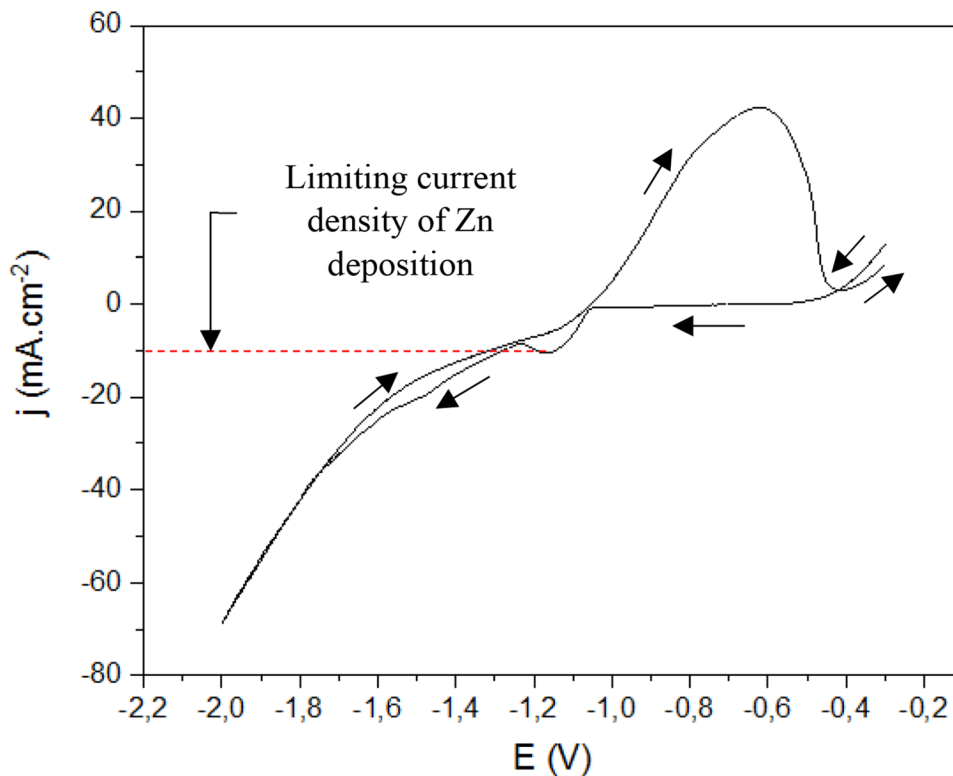
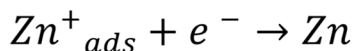
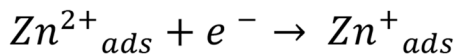
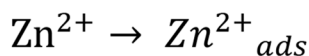
where j (mA cm⁻²): the applied current density and M (g mol⁻¹): molar mass of the substance.

The drop in the CE with increasing the current density is attributed to the HER. However, with higher current densities, the displacement of hydrogen ions by zinc leads to an increase of current efficiency. In fact, the rising hydrogen bubbles may cause an extra convection within a diffusion layer, leading to an enhanced mass transport of zincate ions to an electrode surface, which partially compensates the drop of the current efficiency of the zinc deposition at higher current flows [26, 27].

3.1.3 Microstructural Investigation

3.1.3.1 Morphological Characterization SEM images of investigated Zn coatings are presented in Fig. 5a–d. At a low current density (Fig. 5a), a platelet morphology is observed; the grains have typical hexagonal close-packed crystals, which is a typical morphology of Zn deposits in the absence of additives. The deposit is compact, showing a homogeneous structure which affords a smooth and brilliant aspect. With increasing the current density (Fig. 5b and c), coarse grains, porous and blackish grey deposits are obtained. With higher current density (-40 mA cm^{-2}) a flower-like shape

Fig. 3 Cyclic voltammogram of mild steel in an electrolytic bath containing Zn(II), scan rate = 25 mV s⁻¹



is observed (Fig. 5d), with a transient from bidimensional to tridimensional structure. However, the heterogeneous structure and the random growing of the nanograins provides a dull and rough deposit [5, 16, 27–32].

This result is in accordance with those reported by N. Alias et al. [33], who explained that the change in morphology of Zn deposit from dense and uniaxial to disperse and dendritic was due to the increase in current density used for the deposition.

3.1.3.2 Compositional Analysis (EDS) The EDS analysis shows the elemental composition of Zn deposit on a steel substrate. The spectrum for a deposition at low current density shows a prominent peak of Zn, and noteworthy peaks of O and C (Fig. 6a). The element of carbon mainly comes from the steel substrate, while the oxygen should result from some oxides on the top surface. When we increase the current density, new peaks of K, Cl and even S appeared (Fig. 6b–d) [34–36]. Indeed, the rising hydrogen bubbles may cause an

extra convection within a diffusion layer, inducing K, Cl and S transport and adsorption on the deposit.

Alkire et al. [37] reported that incorporation of sulfur increases with decreasing current density which is in disagreement with our results. Wasekar et al. [38] suggest that, sulfur (S) and carbon (C) adsorb on the crystallographic surface before being incorporated in the coating. The results of the chemical composition of the obtained coatings are presented in Table 3. They show the average value of four measures.

3.1.4 Corrosion Study

In order to produce zinc electrodeposits of 20 μm, a deposition time range was investigated.

The current density is inversely proportional to time, so with the purpose of obtaining the same deposit thickness of 20 μm; an increase in current density is accompanied by a decrease in deposition time and vice versa [39]. Table 4

Fig. 4 The evolution of the deposition potential E_d during Zn electrodeposition with different current densities

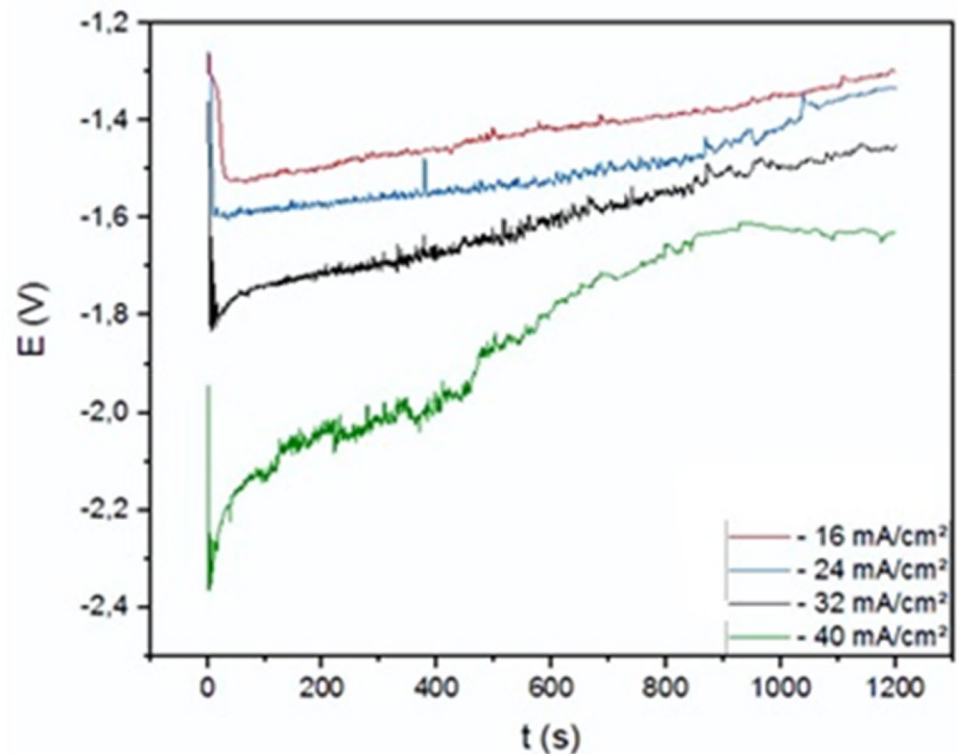


Table 2 Effect of current density on thickness, deposition rate and current efficiency

Current density (j) (mA cm^{-2})	Thickness (e) (μm)	Deposition rate (v) ($\mu\text{m h}^{-1}$)	Current Efficiency (CE) (%)
-16	5.7	17.1	63
-24	6.4	19.2	47
-32	8.8	26.4	46.56
-40	11.7	35.1	52.5

shows the results of the applied current densities and deposition time to have a uniform thickness of $20 \mu\text{m}$ for all the electrodeposited coatings.

3.1.4.1 Measurement of Open Circuit Potentials (OCPs) Figure 7 shows the potential–time dependence for the deposition of zinc on steel substrate at different current densities.

For a current density of -16 and -24 mA cm^{-2} , the OCPs started to decrease and then stabilize to a stable value of -1.055 and -1.071 V , respectively, owing to dezincification. From immersion, the OCP of a current density of -32 mA cm^{-2} , increases towards more noble values characterizing a phenomenon of spontaneous passivation (formation of a passive layer). The potential decreases abruptly towards more electronegative values; it is a rupture of the formed passive layer. Then the potential evolves towards a stationary state with more electronegative values

of -1.097 V , which characterizes a phenomenon of uniform corrosion. For higher current densities, the potential evolves, from immersion, towards more noble values before stabilizing in a value of -1.058 V . This behavior highlights a phenomenon of passivation [40].

3.1.4.2 Polarization Measurements Figure 8 shows the polarization curves of Zn coatings with different current densities in 3.5% NaCl solution. The fitting results of corrosion potential (E_{corr}) and corrosion current density (i_{corr}) obtained from potentiodynamic polarization curves shown in Fig. 8 are summarized in Table 5.

As stated in Table 5, the corrosion current density (i_{corr}), calculated by extrapolation of the curve slopes, increases from $89.98 \mu\text{A.cm}^{-2}$ to $195.59 \mu\text{A.cm}^{-2}$, when the current density is increased from -16 mA.cm^{-2} to -32 mA.cm^{-2} , respectively. Nonetheless, i_{corr} decreases again to $43.75 \mu\text{A.cm}^{-2}$ when the current density reaches a value of -40 mA.cm^{-2} .

The extremely high nucleation rate induced by the high applied overvoltage and the strong hydrogen evolution, gives rise to non-uniform and porous deposits with increasing the current density (Fig. 5). Consequently, the corrosion rate increases with increasing the current density (Table 5).

However, higher current densities (-40 mA cm^{-2}) induces intensive hydrogen evolution. Because of this large amount of hydrogen gas evolved at the cathode surface, hydroxyl ions (OH^-) are abundant at the cathode surface.

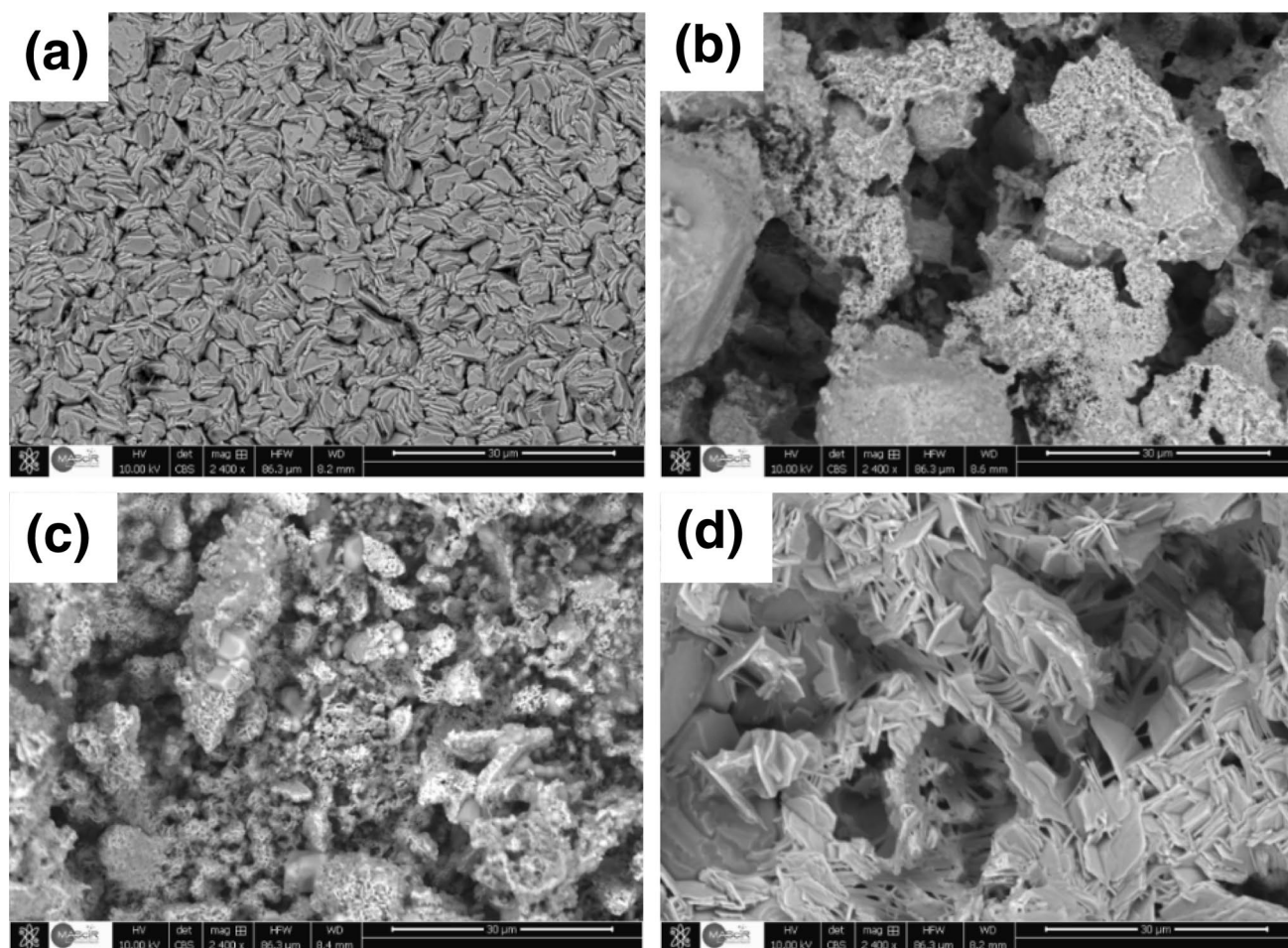
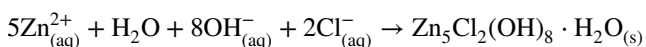
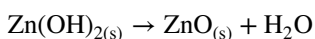
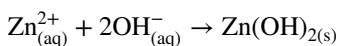
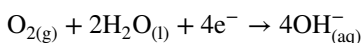


Fig. 5 SEM images of Zn deposit obtained with different current densities: **a** – 16 mA cm⁻², **b** – 24 mA cm⁻², **c** – 32 mA cm⁻² and **d** – 40 mA cm⁻²

Local pH in the vicinity of the cathode surface seems to be much higher than the bulk solution pH, leading to a quick alkalization of the metal/solution interface [2, 41, 42]. The hydroxide film is the basis for further growth of corrosion products. According to Rahsepar et al. [43] and Yadav et al. [44], possible corrosion products of zinc are reported compounds such as ZnO, Zn(OH)₂, ZnCO₃, Zn₅(OH)₆(CO₃)₂ (hydrozincite) and Zn₅(OH)₈Cl₂·H₂O (simonkolleite), according to [14, 45]:



The formation of Zn corrosion products is the responsible for the drop in the corrosion rate at high current density (–40 mA cm⁻²).

The cathodic polarization curve previously presented for Zn²⁺/Zn reaction on steel (Fig. 8) showed an “elbow turn”, that emerged due to the corrosion of the zinc previously deposited [41].

3.1.4.3 Electrochemical Impedance Spectroscopy Though potentiodynamic polarization technique is used to study the kinetics of an electrode reaction, the result is often corrupted by side effects such as the charging currents of the double layer observed on a time-scale of the order of a millisecond, or by the ohmic drop associated to the experimental setup. The response of reversible electrochemical systems studied in the presence of an ohmic drop unfortunately resembled the response of kinetically slow systems. The best way of differentiating the kinetics of an electrode reaction from experimental side effects is to use an excitation function covering a large time domain. Thus, EIS was used to evaluate the bar-

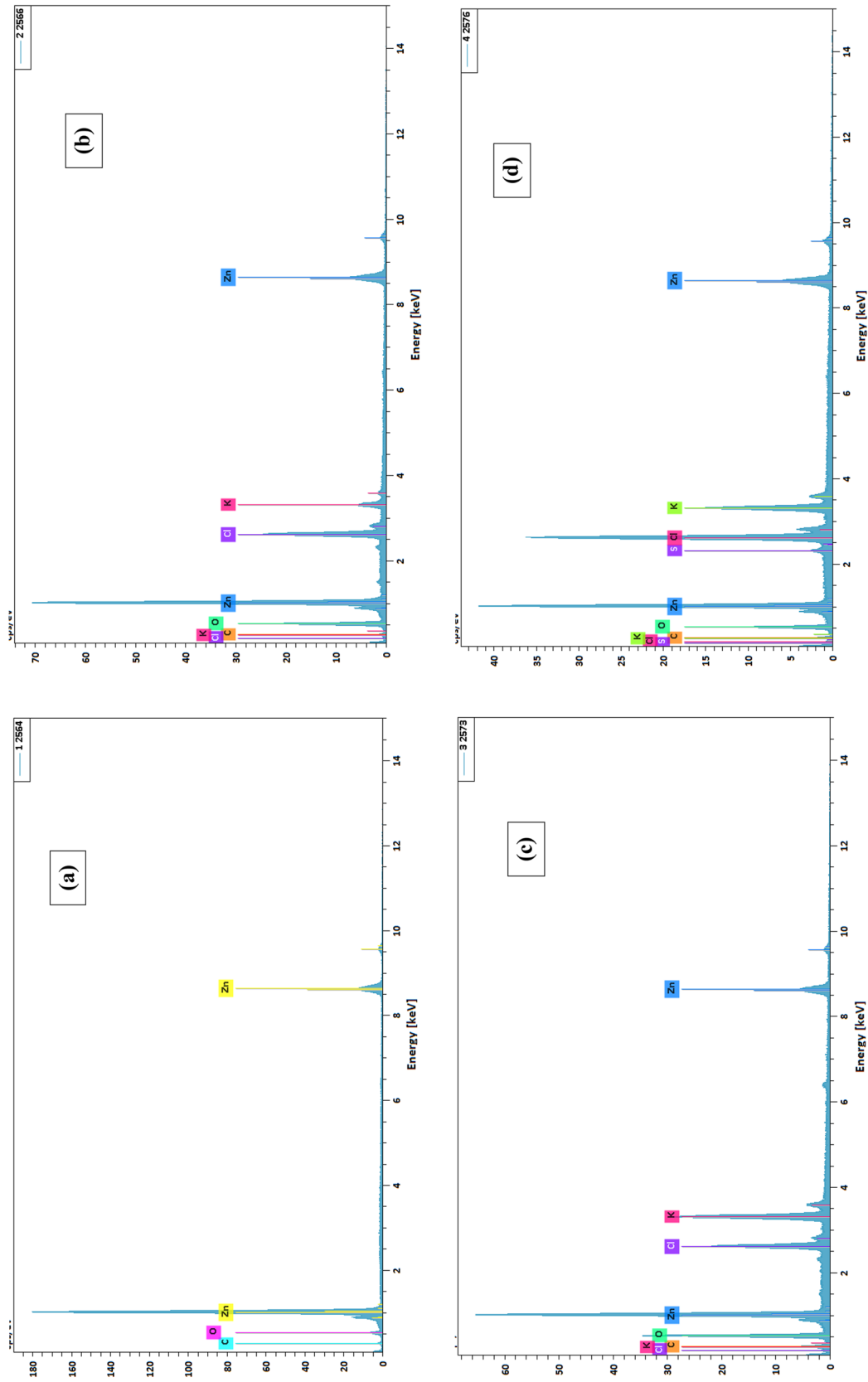


Fig. 6 EDS analysis of the Zn coating obtained with different current densities: **a** – 16 mA cm⁻², **b** – 24 mA cm⁻², **c** – 32 mA cm⁻² and **d** – 40 mA cm⁻²

Table 3 Chemical composition of the obtained deposit at different current densities

Current density (mA cm ⁻²)	C (%)	O (%)	S (%)	Cl (%)	K (%)	Zn (%)
-16	15.81	11.26	-	-	-	72.92
-24	8.55	38	-	14.1	3.25	35.6
-32	9.02	34.03	1.02	7.31	11.66	36.95
-40	6.50	15.42	7.52	21.88	24.35	24.31

rier properties of the electrical double layer capacitance and to determine the polarization resistance [46].

Figure 9 shows Nyquist plots of impedance response obtained in 3.5% NaCl solution with different current densities. Where $Z_r(\omega)$ and $Z_{im}(\omega)$ are the real and imaginary parts of the measured impedance, respectively, and ω is the angular frequency.

A semicircle aspect is first observed in the Nyquist plot, followed by a straight line whose tangent to the real axis is 45°, which is related to a Warburg diffusion process [47], i.e., when the kinetic process is not the determinant in the electrodeposition process, Warburg impedance occurs, which is the result of ion diffusion through micro pores in the coating. In this case, Warburg impedance represents the diffusion of oxygen from the electrolyte to the pores of zinc [47–52].

Electrochemical impedance spectroscopy (EIS) has become a very important tool in the analysis of corrosion and essentially all electrochemical phenomena [53]. However, for more accuracy of Zn coatings corrosion behavior, Bode plots are presented in Fig. 10.

Bode plots reveal two peaks, one in the high- and one in the low-frequency range. As the phase angles tend to -90°, but they do not reach to that value, it can be concluded that CPE (Constant Phase Element) behavior is present at the interface. Deviation from pure capacitance can be a result of surface roughness, cracks, porosities or variation of chemical composition [14, 54].

In the evaluation of impedance data, the electrochemical interphase is often described by an equivalent circuit suited for the conditions of the experiment, using circuit elements that represent the various existing physical processes [53]. The electrical EC employed to fit the EIS data for the electrodeposited coatings are shown in Fig. 11. In

these equivalent circuits R_s is the solution resistance, Q_c is the capacitance of the coating, R_c is the resistance of the porous layer, R_{ct} is the charge transfer resistance, and Q_{dl} is the double layer capacitance. The impedance of CPE is defined as:

$$Z_{CPE} = 1/Y_0(j\omega)^n$$

where Y_0 is general admittance function (sⁿ/ohm) and it is connected with active surface area of the coatings, ω is angular frequency (rad/s), and n is a coefficient related to deviation between real and pure capacitance and can be used as a measure of the surface inhomogeneity. The n value is varied in the range of -1 to 1, where -1, 0 and 1 depict CPE as effective inductor, ideal resistance and pure capacitor, respectively. The n value for porous coatings can be equal to 0.5 [14]. The corresponding EIS parameters are analyzed and listed in Table 6.

Where $R_1 = R_s$, $Q_1 = Q_c$, $R_2 = R_c$, $Q_3 = Q_{dl}$ and $R_3 = R_{ct}$.

As seen in Table 6, the values of charge transfer resistance R_{ct} decreases from 6.75 Ω cm² for a current density of -16 mA cm⁻², to 4.68 Ω cm² for a current density of -32 mA cm⁻², respectively. This could be associated to the dissolution of new and unstable corroded surface areas, while for a current density of -40 mA cm⁻², the increase in R_{ct} value indicates that the active area became totally covered by precipitated corrosion products (zinc oxides and hydroxides), which was demonstrated earlier, owing to the OCP plots, approving a phenomenon of passivation for -40 mA cm⁻². The increase in Q_{dl} indicates a less compact and less stable layer. The polarization resistance R_p ($R_p = R_c + R_{ct}$) of the studied specimens decreases from 36.80 Ohm cm² for -16 mA cm⁻² to 28.87 Ohm cm² for -24 mA cm⁻², 17.92 Ohm cm² for -32 mA cm⁻² and rises again to 74.26 Ohm cm² for -40 mA cm⁻². The polarization resistance is inversely proportional to the corrosion rate. Thus, good agreement was obtained between EIS measurements and the potentiodynamic polarization results, indicating an increase in the corrosion rate with current density and then a drop in its value with higher current densities, because of the formation of oxide/hydroxide Zinc products [54–56]. In the next section, a deposition current density of -16 mA cm⁻² will be used.

Table 4 The applied current densities and deposition time for a uniform thickness for all electrodeposited coatings

Current density (mA cm ⁻²)	Deposition time (min)	Thickness (µm)
-16	30	20.7
-24	29	21.5
-32	28	22.5
-40	20	20

Fig. 7 The potential–time dependence for the deposition of zinc on steel substrate at different current densities

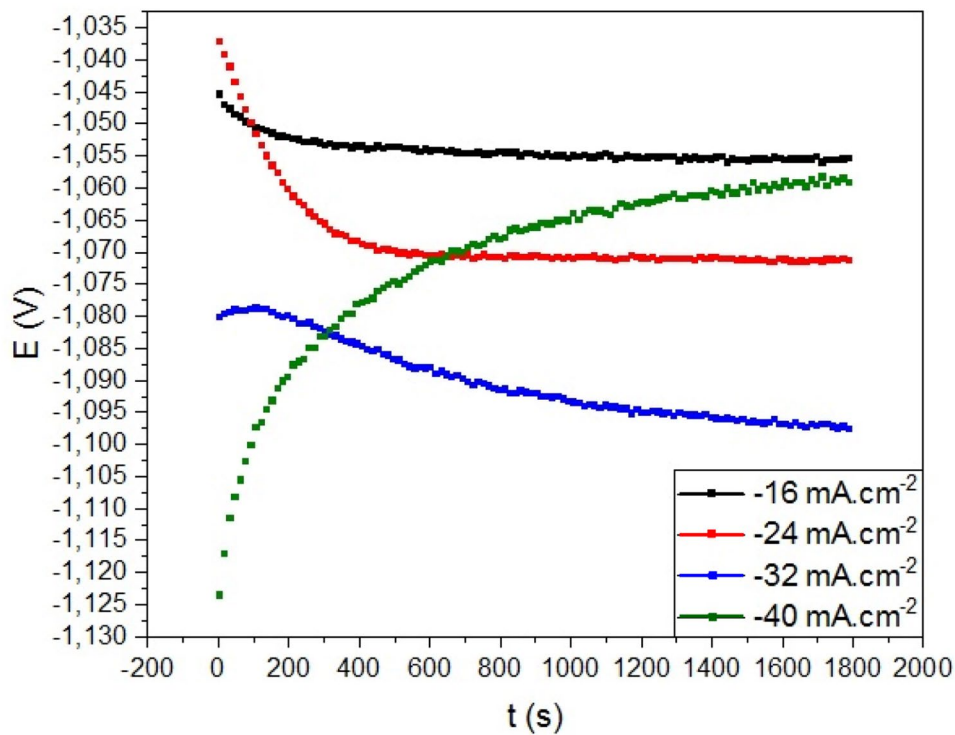


Fig. 8 Polarization measurements of Zn coatings with different current densities in 3.5% NaCl

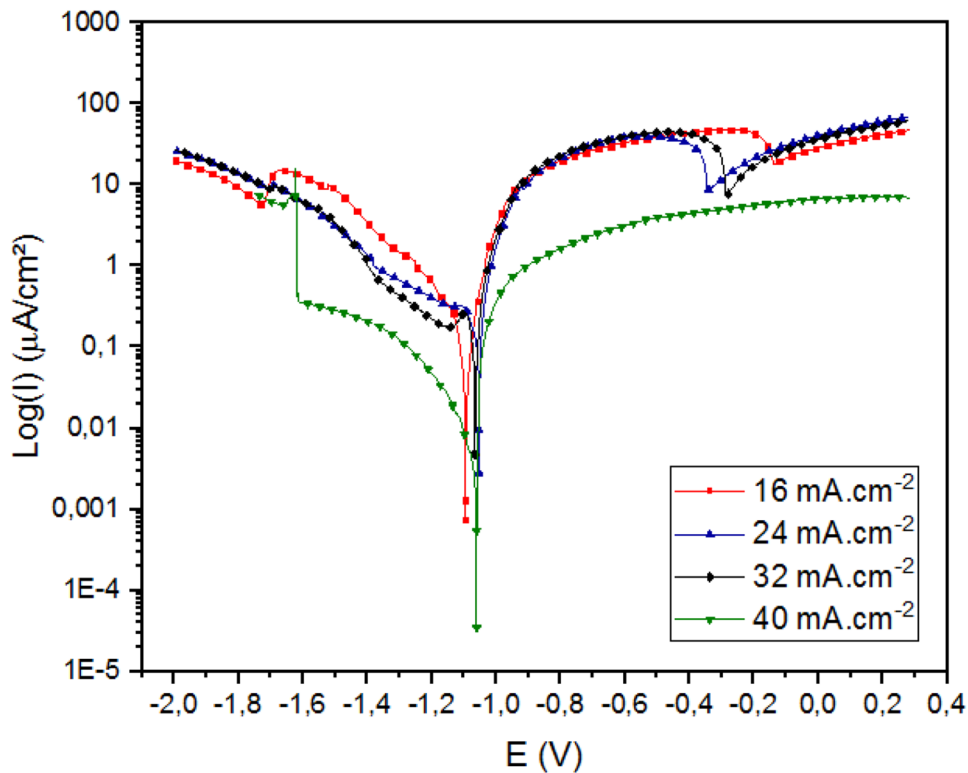


Table 5 Fitting parameters for Tafel plots for Zn coatings with different current densities

Current density (mA cm ⁻²)	<i>i</i> _{corr} (μA cm ⁻²)	<i>E</i> _{corr} (mV)
-16	89.98	-1052.87
-24	105.77	-1132.27
-32	195.59	-1086.04
-40	43.75	-1107.80

3.2 Effect of pH on Zn Deposition

3.2.1 Voltammetric Study

Figure 12 shows the voltamogram of deposition and dissolution of zinc at different pH values. It is clear that we have a single anodic peak around -500 mV, which corresponds to the anodic dissolution of Zinc. In the cathodic

Fig. 9 Nyquist plots of impedance response obtained in 3.5% NaCl solution with different current densities

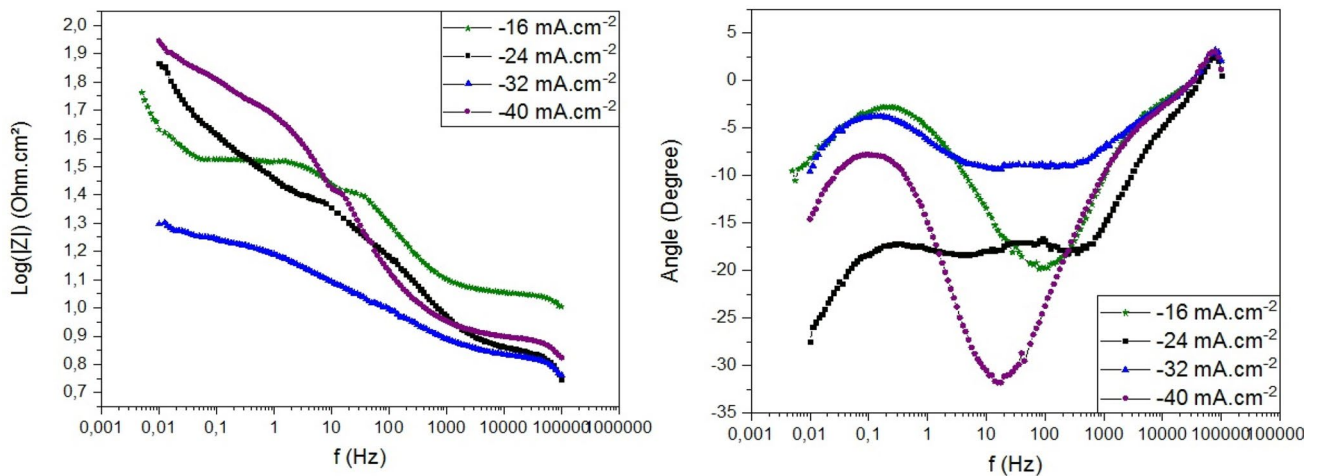
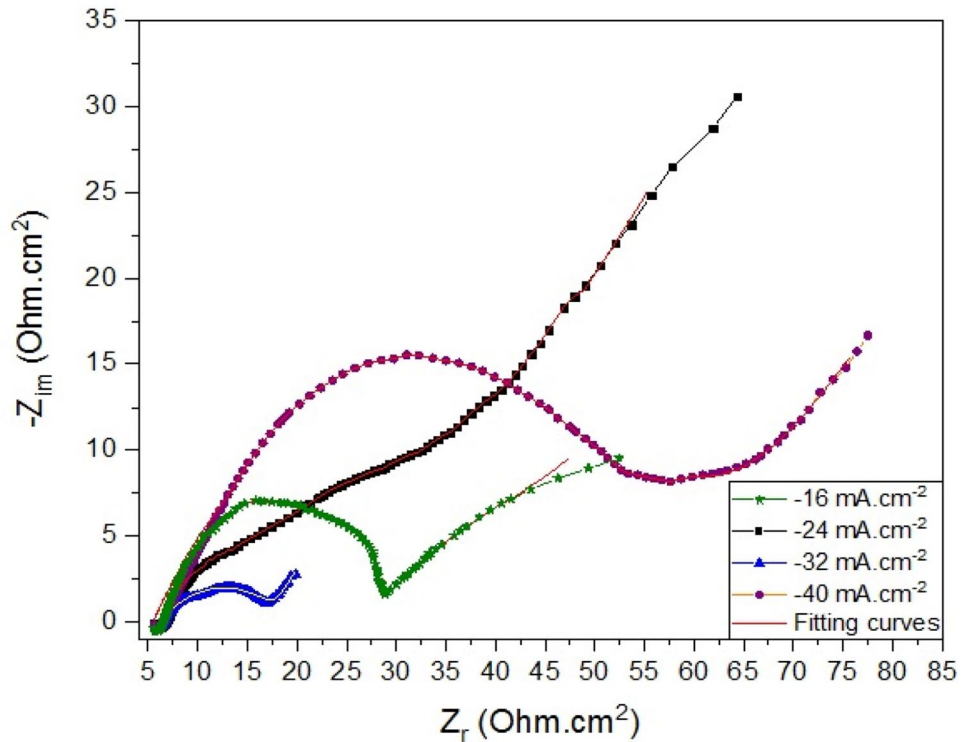


Fig. 10 Bode plots for Zn coatings in 3.5% NaCl with different current densities

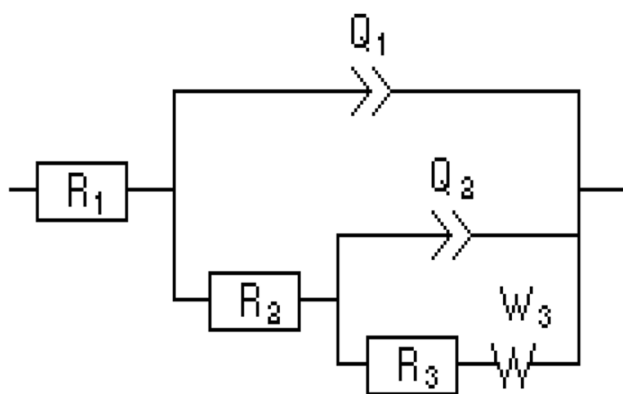


Fig. 11 EC for electrodeposited Zn coatings in 3.5% NaCl at various current densities

scan, we notice that all cathodic peaks start around -1.12 V, except for the voltamogram with a pH of 1.4, where we note the presence of a first cathodic peak that starts roughly at -700 mV and then a 2nd that starts approximately at -1.12 V.

Furthermore, we note the shift of the galvanostatic curves towards higher values of cathodic potentials with increasing pH, witnessing of the complexity of electroplating with pH.

In order to know the origin of the cathodic peaks, we carried out several experiments. First of all, we prepared a bath without $ZnSO_4$, to identify the peaks related to zinc deposition (Fig. 13).

We note that all the peaks have faded from the voltamogram, except for the cathodic peak, at around -700 mV. Thus, all other peaks in the cathodic zone are related to zinc deposition. The peak at -700 mV is probably due to the HER (Hydrogen Evolution Reaction), because it disappears with raising the pH values. To confirm this hypothesis, many experiments were conducted.

We note only the presence of hydrogen evolution, in the electrolytes (a) and (b) of Fig. 14. Nonetheless, when KCl is added, the cathodic peak at -700 mV emerges again (Fig. 14c, d).

Accordingly, we conclude that the peak at -700 mV is maybe due to the presence of impurities in KCl.

In the presence of zinc, the amplitude of the peak and hydrogen evolution decrease with the pH, because of the

competitive adsorption between Zn^{2+} ions, H^+ and the impurities present in KCl.

3.2.2 Gravimetric Study

Figure 15 shows the variation of the deposition potential as a function of the bath pH. At lower pH values, deposition takes place with a weak nucleation overpotential than that required for higher pH values. Over long periods, deposition potential is found to increase towards a growth potential characteristic of an increase in Zn content.

When the pH is increased to 5.5, the galvanostatic curves shift to more cathodic potentials, proving that the decrease in pH usually leads to a decrease in the cathodic deposition potential, as well as a decrease in its overvoltage, thus facilitating the deposition process. However, at high pH values, a strong overvoltage is required to create the first nuclei [57].

Table 7 shows the variation of the thickness, the deposition rate and the current efficiency with different pH values. We note that the thickness and the current efficiency decrease with the pH fall. This is probably due to the weak charge transfer and the vigorous HER at low pH values. This result is similar to that reported by Boiadjieva et al. [21], which states a change in the current efficiency from 98% at pH 5.4 to 88% with pH 1.0, with a current density of 100 mA cm^{-2} .

3.2.3 Microstructural Investigation

3.2.3.1 Morphological Characterization Changes in the morphology of deposits as a function of pH are presented in Fig. 16. We note the formation of circular grains, uniformly distributed, at a pH of 1.4. However, it is found that the deposit suffers from the presence of multiple holes and voids, certainly due to the intense hydrogen evolution at a low pH value. The morphology changes into needle structure, characterizing an early two-dimensional growth of the germs formed. Given the basic nucleation theory and growth process [57], it is realized that nucleation and growth rate are potentially dependent. The deposit becomes compact and homogeneous at a pH of 4.5, in the form of hexagonal plates, uniformly distributed, giving rise to a smooth and shiny appearance. The structure

Table 6 Equivalent circuit parameters of Zn coatings with different current densities

j (mA cm^{-2})	R_s ($\Omega \text{ cm}^2$)	Q_c ($\mu\text{F cm}^2$)	n_c	R_c ($\Omega \text{ cm}^2$)	Q_{dl} ($\mu\text{F cm}^2$)	n_{ct}	R_{ct} ($\Omega \text{ cm}^2$)	W ($\Omega \text{ s}^{-1/2}$)	R_p ($\Omega \text{ cm}^2$)
-16	10.75	1.45	0.61	30.05	7.65	0.47	6.75	1.53	36.80
-24	6.49	1.04	0.62	13.96	0.01	0.73	14.91	8.59	28.87
-32	6.05	0.01	0.37	13.24	5.62	0.97	4.68	0.79	17.92
-40	7.49	3.05	0.59	54.73	0.18	0.47	19.53	14.3	74.26

Fig. 12 Voltamogram of deposition and dissolution of zinc at different pH values

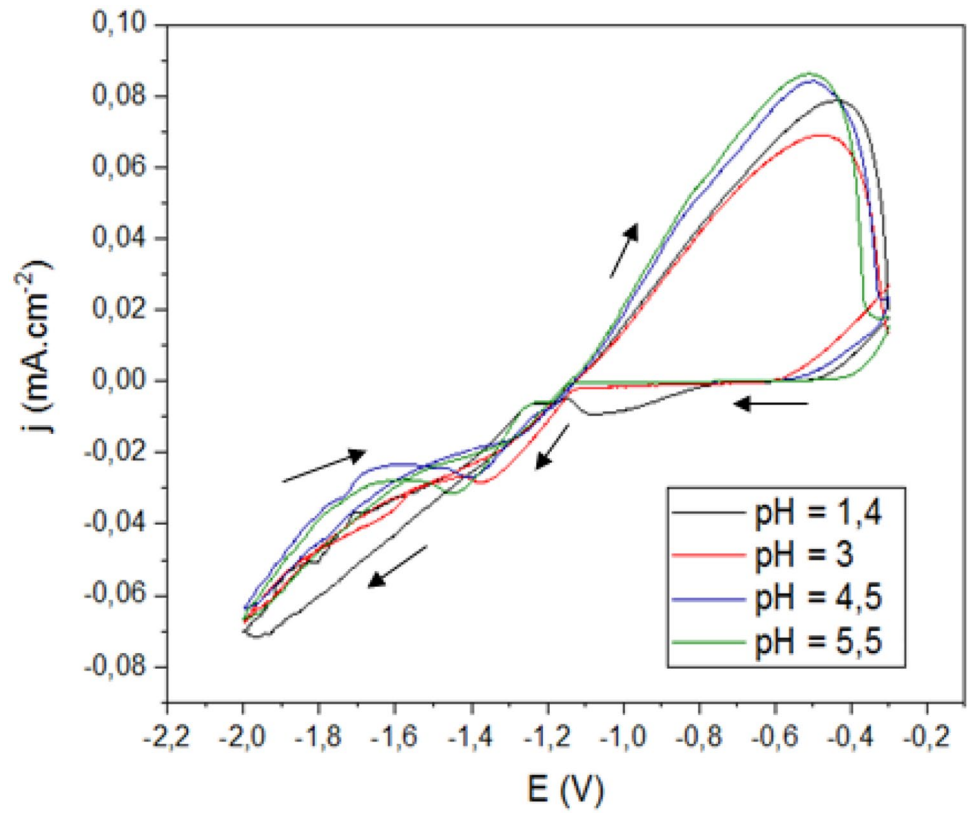


Fig. 13 Steel voltamogram in a sulphate-free bath with different pH values

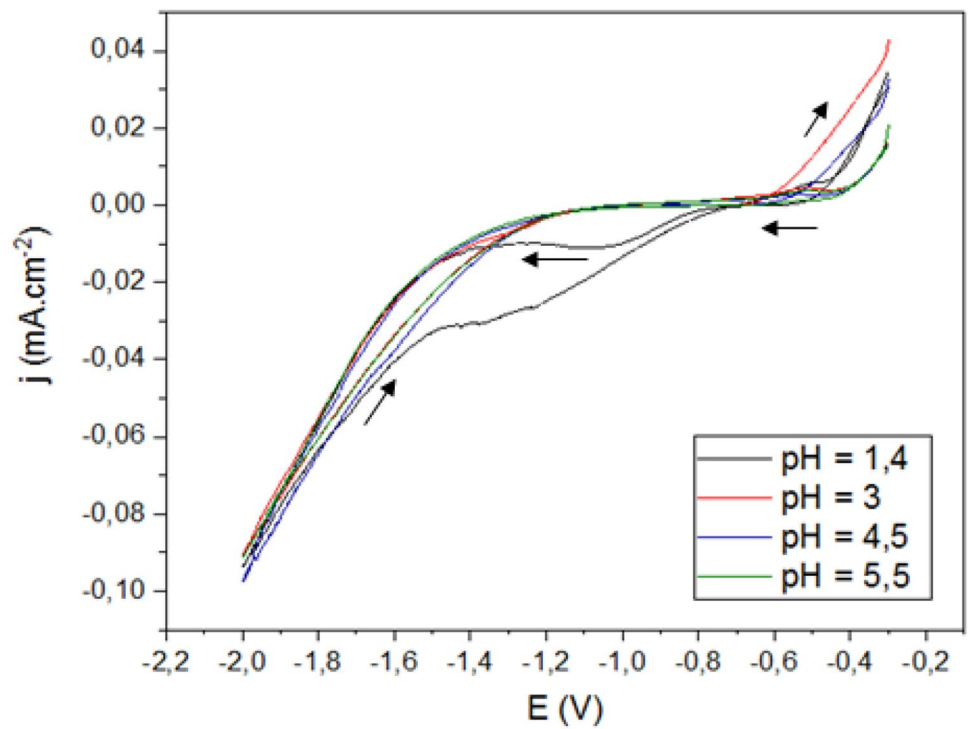
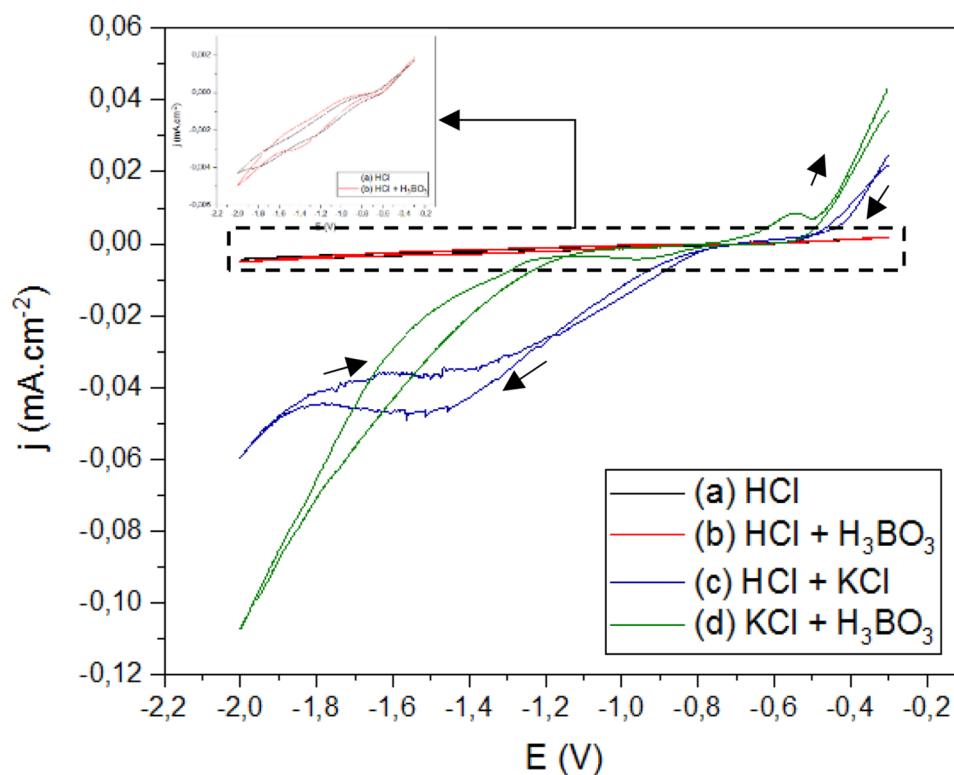


Fig. 14 Steel voltamogram in **a** HCl, **b** HCl+H₃BO₃, **c** HCl+KCl and **d** KCl+H₃BO₃. Zoom in: HER in electrolyte **(a)** and **(b)**



becomes even more compact at a pH of 5.5. Nevertheless, the deposit becomes rough, probably because of the presence of corrosion products.

3.2.3.2 Compositional Analysis (EDS) The EDS analysis shows the elemental composition of Zn deposit on a steel substrate. The EDS spectra of Zn deposition obtained with different pH values are shown in Fig. 17, while the chemi-

Fig. 15 The variation of the deposition potential as a function of the pH bath

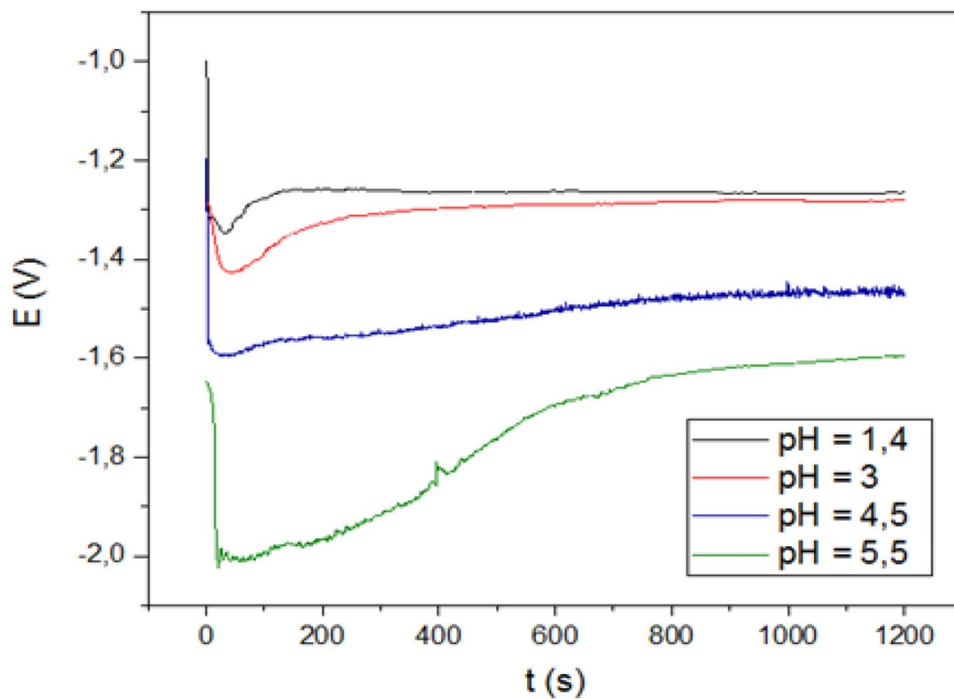


Table 7 Variation of the thickness, the deposition rate and the current efficiency with different pH values

pH	Thickness (<i>e</i>) (μm)	Deposition rate (<i>v</i>) (μm h ⁻¹)	Current efficiency (CE) (%)
1.4	4.1	12.3	46.13
3	4.3	12.9	47.23
4.5	5.7	17.1	63
5.5	5.84	17.52	63.07

cal composition of the elaborated deposits is illustrated in Table 8.

Examining the EDS analysis spectra (Fig. 17) and the chemical composition

(Table 8) of zinc deposits elaborated at different pH values. We note the presence of Fe with a lower %wt at a pH of 1.4 and 3, which probably emanates from the steel substrate, given the presence of notable voids and holes in these deposits. The O content is higher in the developed deposits at a pH of 1.4, 3 and 5.5. This is due to the fact that oxygen

comes mainly from absorbed air (Fig. 17a, b) or in the form of zinc oxide ZnO (Fig. 17d). The deposit produced at a pH of 4.5 (Fig. 17c) contains the least impurities and the highest Zn content.

3.2.4 Corrosion Study

In the following parts, a uniform thickness of 20 μm was produced, by varying the deposition time for each sample.

3.2.4.1 Measurement of Open Circuit Potentials (OCPs)

The open circuit potential measurements of Zn electrodeposited coatings, with different pH values, are shown in Fig. 18.

For a pH range from 1.4 to 4.5, the potential evolves towards more electronegative values characterizing a phenomenon of spontaneous dissolution before stabilizing after a certain time of immersion in the corrosive solution. However, for a pH value of 5.5, the potential evolves, from immersion, towards more noble values before stabilizing in a value of -1.11 V. This behavior highlights a phenomenon of passivation [40].

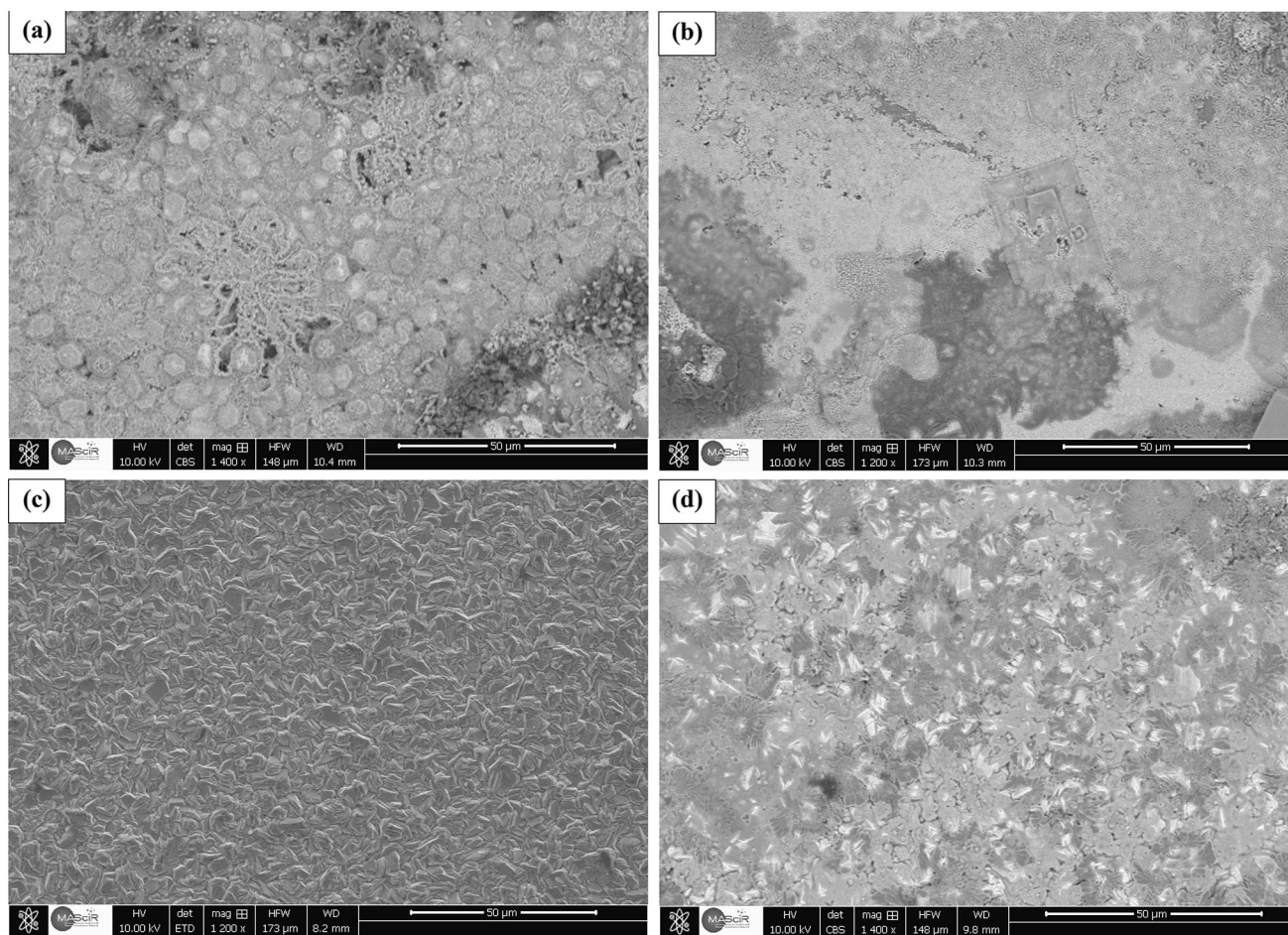


Fig. 16 SEM images of Zn deposit obtained with different pH values: **a** 1.4, **b** 3, **c** 4.5 and **d** 5.5

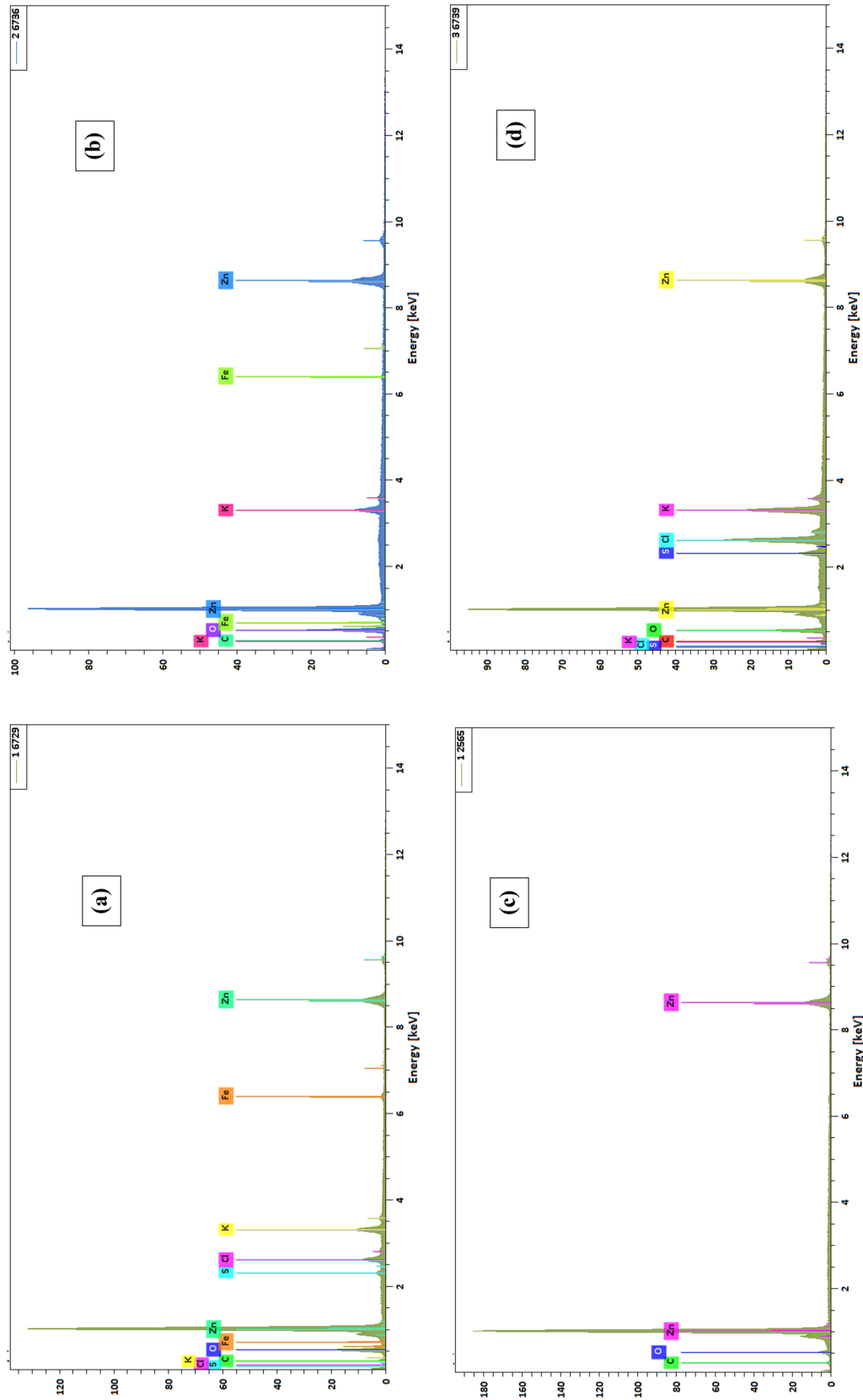


Fig. 17 EDS analysis of the Zn coating obtained with different pH values: **a** 1.4, **b** 3, **c** 4.5 and **d** 5.5

Table 8 Chemical composition of the obtained deposit at different pH values

pH	C (%)	O (%)	Fe (%)	S (%)	Cl (%)	K (%)	Zn (%)
1.4	5.84	26.80	0.59	4.86	8.61	10.34	42.94
3	8.82	41.61	0.79	0.35	2.28	3.84	42.28
4.5	15.81	11.26	–	–	–	–	72.92
5.5	7.92	21.55	0.13	1.43	12.24	10.56	46.16

Fig. 18 OCP measurements of Zn coatings with different pH values

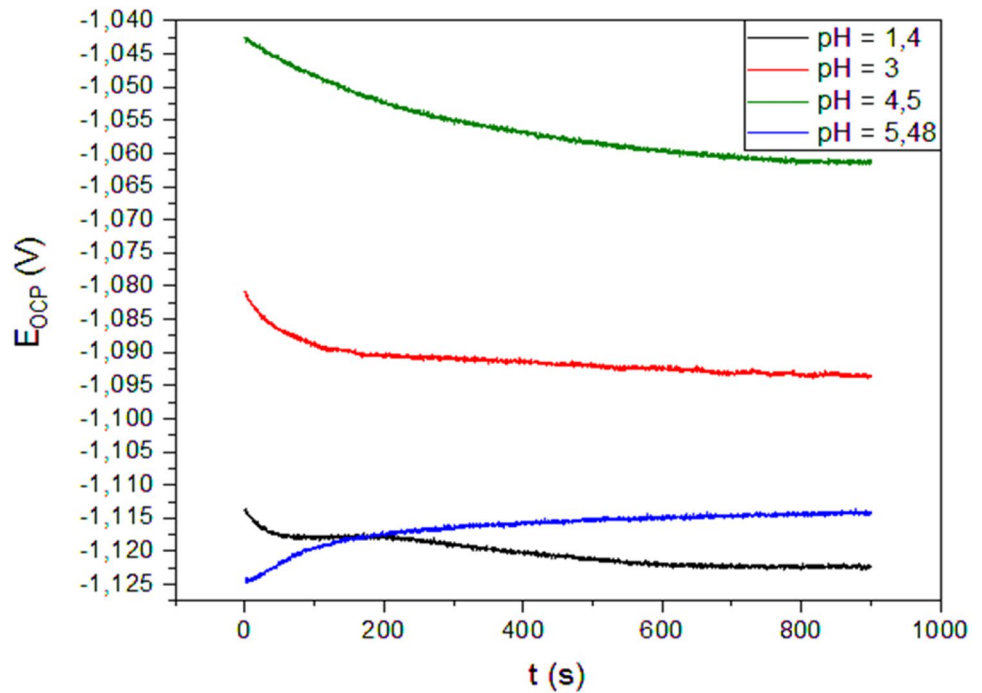


Fig. 19 Tafel plots of Zn coatings with different pH values in 3.5% NaCl solution

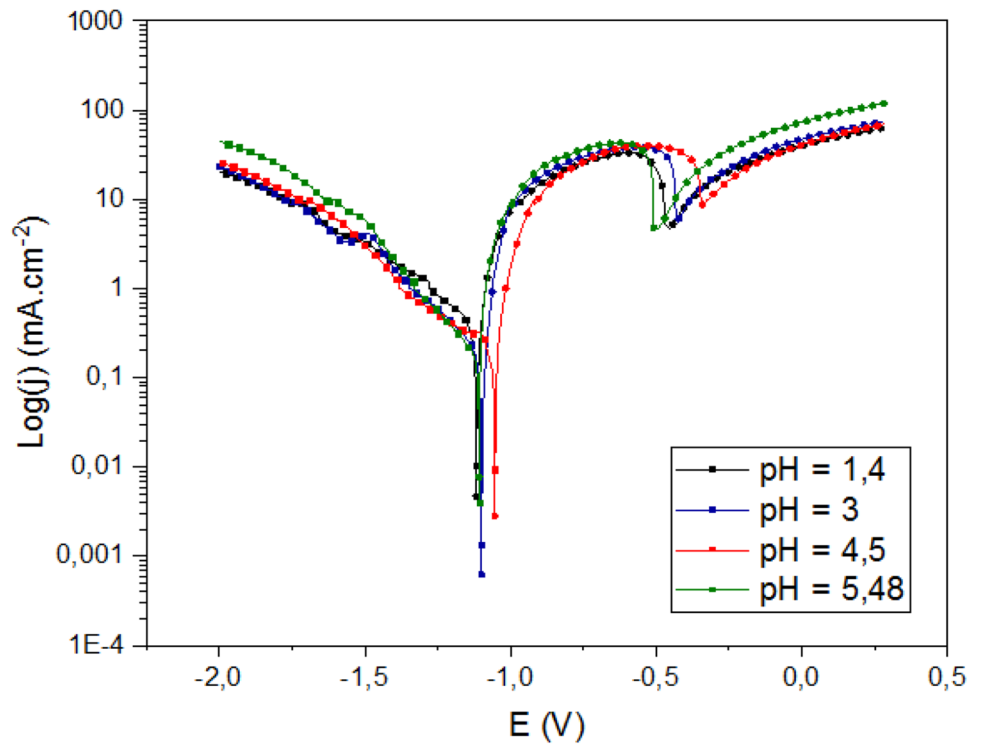


Table 9 Fitting parameters for Tafel plots for Zn coatings with different pH values

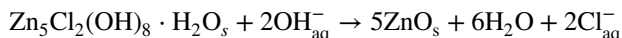
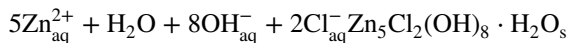
pH	i_{corr} (Ma cm^{-2})	E_{corr} (mV)
1.4	94.77	-1117.67
3	91.77	-1097.21
4.5	89.98	-1052.87
5.5	77.26	-1106.91

The OCP measurements provide qualitative information on the spontaneity of the metal to corrode and do not quantify the corrosion rates [3, 41]. For more accuracy, the determination of the corrosion current (i_{corr}) is important.

3.2.4.2 Polarization Measurements Figure 19 shows the polarization curves of Zn coatings with different pH values in 3.5% NaCl solution. The fitting results of corrosion potential (E_{corr}) and corrosion current density (i_{corr}) derived from potentiodynamic polarization curves are shown in Fig. 19 and are summarized in Table 9.

It is ascertained that i_{corr} decreases from 94.77 to 77.26 $\mu\text{A cm}^{-2}$ when the pH increases from 1.4 to 5.5, respectively. The decline in i_{corr} value indicates the decrease in the corrosion rate, which is a result of the formation of hydroxide zinc products as far as we increase pH

values. Linddtröm et al. [58] has reported that simonkolleite ($\text{Zn}_5\text{Cl}_2(\text{OH})_8 \cdot \text{H}_2\text{O}_s$) precipitates when solutions containing zinc ions and chloride ions are neutralized, according to the following reaction:



As published by Linddtröm et al. in Fig. 20, the stability diagram illustrates this.

As the pH increases in the range of 1.4–4.5, the corrosion potentials E_{corr} become more anodic, indicating a facility in the deposition process, this is maybe due to the attenuation of HER with increasing pH. However, at a pH of 5.5, the corrosion potential decreases again, attesting of the complexity in the electrodeposition, which can be related to the formation of hydroxide zinc products at higher pH values. This tendency in the corrosion potentials is confirmed by the Zinc content in Table 8; we note an increase in Zn content in the range of 1.4–4.5 and then a decrease of its %wt at pH 5.5.

As a result of the discussion in Sect. 2.2.3, it is obvious that the minimal corrosion rates match the highest Zinc content in the coating. The coatings developed at lower pH values exhibit higher corrosion rate because of their higher level of porosity.

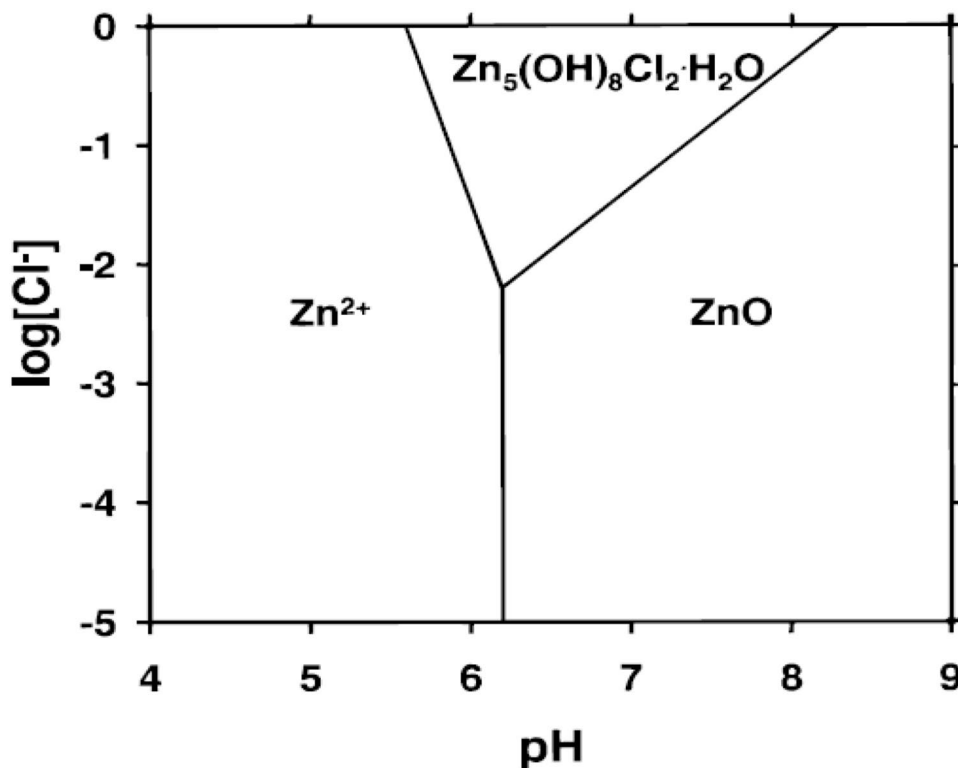
Fig. 20 Stability diagram, $[\text{Zn}^{2+}] = 0.1 \text{ M}$ at 25 °C [58]

Fig. 21 Nyquist plots of impedance response obtained in 3.5% NaCl solution with different pH values

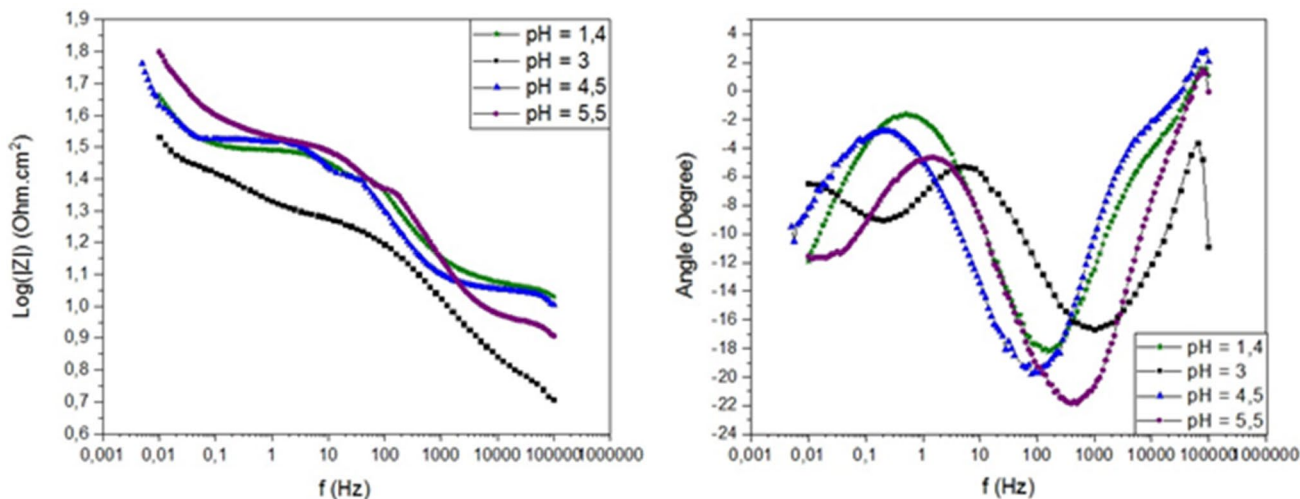
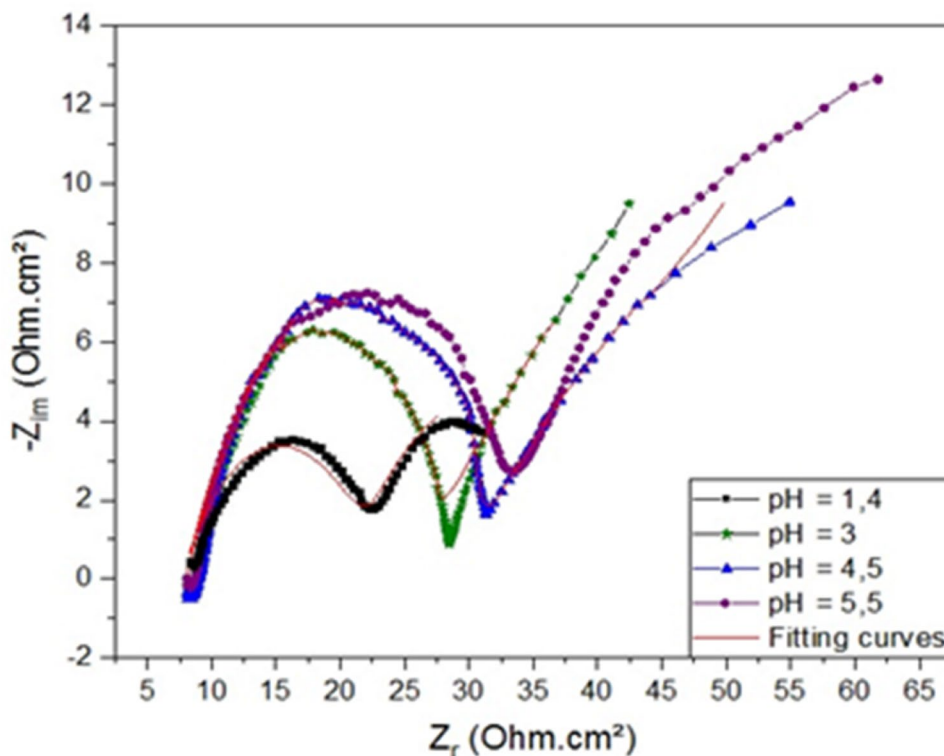


Fig. 22 Bode plots for Zn coatings in 3.5% NaCl with different pH values

3.2.4.3 Electrochemical Impedance Spectroscopy EIS is a useful technique for ranking coatings, assessing interfacial reactions, quantifying coating breakdown, and predicting the lifetime of coating/metal systems [54]. Nyquist plots of impedance response obtained in 3.5% NaCl solution are displayed in Fig. 21.

The Nyquist plots of the Zn coatings studied exhibit a semicircle at higher frequencies, followed by a straight line whose tangent to the real axis is 45°. The semicircle

is related to electrical double layer, forming between the coating and the electrolyte [14]. The diameter of the semicircle is sharply increased with the gradual increase in pH values, indicating a much higher corrosion resistance of the coatings. The straight line is related to a Warburg diffusion process, i.e., when the kinetic process is not the determinant in the electrodeposition process, Warburg impedance occurs, which is the result of ion diffusion through micro pores in the coating. At a pH 1.4, the coating is porous (Fig. 16a),

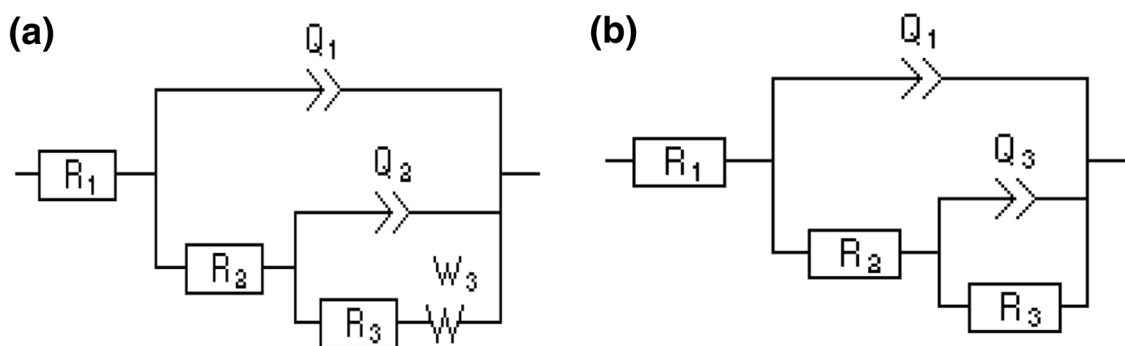


Fig. 23 EC for electrodeposited Zn coatings in 3.5% NaCl at various pH values **a** 1.4, **b** 3, 4.5 and 5.5

Table 10 Equivalent circuit parameters of Zn coatings with different pH values

pH	R_s ($\Omega \text{ cm}^2$)	Q_c (F.S.n ⁻¹)	n_c	R_c ($\Omega \text{ cm}^2$)	Q_{dl} (F.S.n ⁻¹)	n_{ct}	R_{ct} ($\Omega \text{ cm}^2$)	W ($\Omega \text{ s}^{-1/2}$)	R_p ($\Omega \text{ cm}^2$)
1.4	5.175	1.17	0.53	15.12	0.08	0.72	9.25	1.95	24.37
3	11.13	1.10	0.61	20.36	0.37	0.55	12.42	2.4	32.78
4.5	10.75	1.45	0.61	30.05	7.65	0.47	6.75	1.53	36.80
5.5	8.2	0.74	0.59	32.24	4.1	0.49	6.42	4.9	38.66

The pH increase causes the thermodynamic instability of simonkolleite, thus forming zincite

hence this is diffusion through a film. With increasing the pH values to 3 and 4.5, the coating is more uniform and the Warburg impedance represents the diffusion of oxygen from the electrolyte to the pores of zinc (Table 8) [47–51]. At a pH of 5.5, we note the presence of a first loop at high frequencies, which is related to charge transfer resistance in parallel with double layer capacitance, followed by a second incomplete loop at medium frequencies, which can be related to a non-faradic process and then the Warburg impedance because of oxygen diffusion into the coating.

Where $R_1 = R_s$, $Q_1 = Q_c$, $R_2 = R_c$, $Q_3 = Q_{dl}$ and $R_3 = R_{ct}$.

Bode plots (Fig. 22) reveal the presence of two steps at Bode diagrams and two peaks at Bode-phase diagram of the Zn coatings, indicating the presence of two-time constants in these samples. Therefore, the equivalent circuit proposed for Zn coatings, with different pH values, has two-time constants (Fig. 23). The corresponding EIS parameters are analyzed and listed in Table 10.

The solution resistance (R_s) was nearly identical in all cases as the same bath chemistry and cell configuration were used. The value of the polarization resistance (R_p) is higher for zinc electrodeposited at pH 5.5 than at pH 1.4. The increase in the polarization resistance at pH 5.5 is due to the formation of a resistive layer of ZnO. The EIS data are very compatible with the potentiodynamic polarization measurements, showing an increase in the corrosion resistance with pH.

From the results above, it may be concluded that the deposit developed at a pH of 4.5 is the one that contains the least impurities, the highest Zn content and provides a good corrosion resistance.

4 Conclusion

In the present research, a free-additive bath has been used, and Zn electrodeposited coatings have been obtained using different current densities and pH values. The main conclusions drawn from this study are as follows:

- The intensive HER leads to the increase of the corrosion rate with increasing the current density.
- The deposition current density significantly affects the surface morphology and corrosion resistance, due to the incorporation of Zn hydroxide inclusions at higher current densities.
- The voltammetric study revealed that with higher pH values, a high overvoltage is required to create the first nuclei, because of the complexity of electrodeposition.
- The corrosion study showed an increase in the polarization resistance with increasing pH, because of the formation of oxide/hydroxide zinc products with higher pH values.
- The deposit realized at a current density of 16 mA cm^{-2} and a pH of 4.5 contains the least impurities, the highest Zn content and provides a good corrosion resistance.

Compliance with Ethical Standards

Conflict of interest The authors have declared no conflict of interest.

Human and Animal Rights This article does not contain any studies with human or animal subjects.

References

- Ortiz-Aparicio JL, Meas Y, Chapman TW, Trejo G, Ortega R, Chainet E (2015) Electrodeposition of zinc in the presence of quaternary ammonium compounds from alkaline chloride bath. *J Appl Electrochem* 45:67–78
- Loukil N, Feki M (2017) Electrodeposition of Zn–Mn alloy coatings deposited from acidic chloride baths: effect of deposition conditions on the Zn–Mn electroplating, morphological and structural characterization. *Appl Surf Sci* 410:574–584. <https://doi.org/10.1016/j.apsusc.2017.02.075>
- Sriraman KR, Brahimi S, Szpunar JA, Osborne JH, Yue S (2013) Characterization of corrosion resistance of electrodeposited Zn–Ni Zn and Cd coatings. *Elect Acta* 105:314–323. <https://doi.org/10.1016/j.electacta.2013.05.010>
- de Carvalho MF, Rubin W, Carlos IA (2010) Study of the influence of the polyalcohol mannitol on zinc electrodeposition from an alkaline bath. *J. Appl. Electrochem* 40:1625–1632. <https://doi.org/10.1007/s10800-010-0148-0>
- Yang Y, Liu S, Yu X, Huang C, Chen S, Chen G, Wu QH (2015) Effect of additive on zinc electrodeposition in acidic bath. *Surf Eng* 31:446–451. <https://doi.org/10.1179/1743294415Y.0000000006>
- Feeney R, Kounaves SP (2000) Microfabricated ultramicroelectrode arrays: developments, advances, and applications in environmental analysis. *Electroanalysis* 12:677–684
- Abdallah M, Zaaferany I, Fouda AS, Abd El-Kader D (2012) Inhibition of Zinc Corrosion by Some Benzaldehyde Derivatives in HCl Solution. *J Mater Eng Perf* 21:995–1002
- Rashmi D, Pavithra GP, Praveen BM, Devapal D, Nayana KO, Nagaraju G (2020) Electrodeposition of Zn–Ni Monolithic coatings, characterization, and corrosion analysis. *J Failure Anal Prev* 20:513–522. <https://doi.org/10.1007/s11668-020-00848-3>
- Shibli SMA, Manu R (2017) Tuning of the microstructure and surface topography of hot-dip galvanized coatings. *Comp. Mat. Fin* 3:25–37. <https://doi.org/10.1016/B978-0-12-803581-8.09198-0>
- Shibli SMA, Meena BN, Remya RA (2015) Review on recent approaches in the field of hot dip zinc galvanizing process. *Surf Coat Tech* 262:210–215. <https://doi.org/10.1016/j.surfcoat.2014.12.054>
- Aliofkhaezrai M (2011) Nanocoatings. Size Effect in Nanostructured Films, Springer, Berlin
- Raeissi K, Saatchi A, Golozar MA, Texture Szpunar JA (2004) Surface morphology in zinc electrodeposits. *J Appl Electrochem* 34:1249–1258. <https://doi.org/10.1007/s10800-004-1699-8>
- Rudomilova D, Prosek T, Luckeneder G (2018) Techniques of investigation of hydrogen embrittlement of advanced high strength steels. *Corros Rev* 36(5):413–434. <https://doi.org/10.1515/corrrev-2017-0106>
- Tafreshi M, Allahkaram SR, Farhangi H (2016) Comparative study on structure, corrosion properties and tribological behavior of pure Zn and different Zn–Ni alloy coatings. *Mater Chem Phys* 183:263–272. <https://doi.org/10.1016/j.matchemphys.2016.08.026>
- Tz Boiadjieva-Scherzer, Kronberger H, Fafilek G, Monev M (2016) Hydrogen evolution reaction on electrodeposited Zn–Cr alloy coatings. *J Electroanal Chem* 783:68–75. <https://doi.org/10.1016/j.jelechem.2016.10.059>
- Gomes A, da Silva Pereira MI (2006) Pulsed electrodeposition of Zn in the presence of surfactants. *Elect Acta* 51:1342–1350. <https://doi.org/10.1016/j.electacta.2005.06.023>
- Prestat M, Soares CJ, Lescop B, Rioual S, Holzer L, Thierry D (2018) Cathodic corrosion of Zinc under potentiostatic conditions in NaCl solutions. *Chem Electro Chem* 5:1203–1211. <https://doi.org/10.1002/celec.201701325>
- El-Shafei AA, Taguchi S, Aramata A (2008) Zinc underpotential deposition at Pt(111) and Pt(110) under the influence of boric acid and chloric anions. *Russian J Elect* 44:690–696. <https://doi.org/10.1134/S1023193508060098>
- Boiadjieva T, Monev M, Tomandl A, Kronberger H, Fafilek G (2009) Electrochemical studies on Zn deposition and dissolution in sulphate electrolyte. *J Solid-State Electron* 13:671–677. <https://doi.org/10.1007/s10008-008-0594-3>
- Ohba M, Panossian Z, Camargo P (2013) A study on zinc electrodeposition onto zinc cathode. *Trans IMF* 84:320–325. <https://doi.org/10.1179/174591906X149455>
- Boiadjieva T, Monev M, Tomandl A, Kronberger H, Fafilek G (2009) Electrochemical studies on Zn deposition and dissolution in sulphate electrolyte (2009). *J. of Sol. St. Electrochem* 13:671–677. <https://doi.org/10.1007/s10008-008-0594-3>
- Tena-Zaera R, Elias J, Wang G, Levy-Clement C (2007) Role of chloride ions on electrochemical deposition of ZnO nanowire arrays from O₂ reduction. *J Phys Chem C* 111:16706–16711
- Azevedo MCC, Cavaleiro AMV (2012) The acid-base titration of a very weak acid: boric acid. *J Chem Educ* 89:767–770. <https://doi.org/10.1021/ed200180j>
- Gu P, Zheng M, Zhao Q, Xiao X, Xue H, Pang H (2017) Rechargeable zinc-air batteries: a promising way to green energy. *J Mater Chem. A* 5:7651–7666. <https://doi.org/10.1039/C7TA01693J>
- ElFazazi A, Ouakki M, Cherkaoui M (2019) Electrochemical deposition of Zn on mild steel. *Med J Chem* 8:30–41. <https://doi.org/10.13171/mjc8119021318mo>
- Dundálek J, Šnajdr I, Libánský O, Vrána J, Povedič J, Mazúr P, Kosek J (2017) Zinc electrodeposition from flowing alkaline zincate solutions: role of hydrogen evolution reaction. *J Power Sources* 372:221–226. <https://doi.org/10.1016/j.jpowsour.2017.10.077>
- Elsherie AE (2003) Effects of cobalt, temperature and certain impurities upon cobalt electro-winning from sulfate solutions. *J Appl Electrochem* 33:43–49
- Habekost A (2018) Vanadium redox flow batteries with different electrodes and membranes. *J Chem Educ* 6(1):8–13. <https://doi.org/10.12691/wjce-6-1-2>
- Matienco LI, Mosolova LA, Binyukov VI, Zaikov G (2015) Selective ethylbenzene oxidation with dioxygen in the presence of binary and triple catalytic systems introduced redox inactive metal compound, list, and additives of monodentate ligands-modifiers: dMF, HMPA and PHOH. *Kinet Mech Ox Com* 38(3):1169–1182
- Kwon M, Jo D, Cho SH, Kim HT, Park JT, Park JM (2016) Characterization of the influence of Ni content on the corrosion resistance of electrodeposited Zn–Ni alloy coatings. *Surf Coat Tech* 288:163–170. <https://doi.org/10.1016/j.surfcoat.2016.01.027>
- Raeissi K, Saatchi A, Golozar MA, Szpunar JA (2005) Effect of surface preparation on zinc electrodeposited texture. *Surf Coat Tech* 197:229–237. <https://doi.org/10.1016/j.surfcoat.2004.09.024>
- Leung PK, Ponce-de-Leon C, Low CTJ, Walsh FC (2011) Zinc deposition and dissolution in methane sulfonic acid onto a carbon composite electrode as the negative electrode reactions in hybrid redox flow battery. *Elect Acta* 56:6536–6546. <https://doi.org/10.1016/j.electacta.2011.04.111>
- Alias N, Mohamad AA (2015) Morphology study of electrodeposited zinc from zinc sulfate solutions as anode for zinc-air and

- zinc-carbon batteries. *J King Saud Univ Eng Sci* 27:43–48. <https://doi.org/10.1016/j.jksues.2013.03.003>
34. Sharma A, Jang YJ, Jung JP (2015) Effect of current density on morphology of electroplated tin. *Surf Eng* 31:458–464. <https://doi.org/10.1179/1743294414y.0000000427>
 35. Kong G, Liu L, Lu J, Che C, Zhong Z (2010) Study on lanthanum salt conversion coating modified with citric acid on hot dip galvanized steel. *J Rare Earths* 28:461–465. [https://doi.org/10.1016/S1002-0721\(09\)60134-4](https://doi.org/10.1016/S1002-0721(09)60134-4)
 36. Zhang J, Gu C, Tu J (2017) Potentiodynamical deposition and corrosion behavior of thin Zn-Sn coatings with layered structure and varied composition from deep eutectic solvent. *Surf& Coat Tech* 320:640–647. <https://doi.org/10.1016/j.surfcoat.2016.10.004>
 37. Alkire RC, Kolb DM, Lipkowski J, Ross PN (2008) Electrochemical surface modification thin films, functionalization and characterization. *Electrochemical surface modification: thin films, functionalization and characterization*. Wiley, New York
 38. Wasekar NP, Haridoss P, Seshadri SK, Sundararajan G (2016) Influence of mode of electrodeposition, current density and saccharin on the microstructure and hardness of electrodeposited nanocrystalline nickel coatings. *Surf Coat Tech* 291:130–140. <https://doi.org/10.1016/j.surfcoat.2016.02.024>
 39. Tuaweri TJ, Adigio EM, Jombo PP (2013) A study of process parameters for zinc electrodeposition from a sulphate bath. *Int J Eng Sci* 2:17–24
 40. Fiaud C Inhibiteur de corrosion. *Technique de l'ingénieur, traité métallurgie*
 41. Ohba M, Scarazzato T, Espinosa DCR, Panossian Z (2019) Study of metal electrodeposition by means of simulated and experimental polarization curves: zinc deposition on steel electrodes. *Elect Acta* 309:86–103. <https://doi.org/10.1016/j.electacta.2019.04.074>
 42. Ünal HI, Zor S, Gökeril HM (2013) Corrosion behavior of Zn and Ni coated carbon steels in 3% NaCl. *Prot Met Phys Chem Surf* 49:591–596. <https://doi.org/10.1134/S2070205113050158>
 43. Rahsepar M, Bahrololoom ME (2009) Corrosion study of Ni/Zn compositionally modulated multilayer coatings using electrochemical impedance spectroscopy. *Corr. Sci* 51:2537–2543. <https://doi.org/10.1016/j.corsci.2009.06.030>
 44. Yadav AP, Nishikata A, Tsuru T (2004) Electrochemical impedance study on galvanized steel corrosion under cyclic wet–dry conditions—influence of time of wetness. *Corr Sci* 46:169–181
 45. Dutra CAM, Codaro EN, Nakazato RZ (2012) Electrochemical behavior and corrosion study of electrodeposits of Zn and Zn-Fe-Co on steel. *Mat. Sci. Appl* 3:348–354. <https://doi.org/10.4236/msa.2012.36050>
 46. Yogesha S, Bhat KU, Hegde AC (2011) Effect of current density on deposit characters of Zn-Co alloy and their corrosion behaviors. *Metal-Org Nano-Metal Chem* 41:405–411. <https://doi.org/10.1080/15533174.2011.556409>
 47. Celante VG, Freitas MBJG (2010) Electrodeposition of copper from spent Li-ion batteries by electrochemical quartz crystal microbalance and impedance spectroscopy techniques. *J Appl Electrochem* 40:233–239. <https://doi.org/10.1007/s10800-009-9996-x34>
 48. Wang L, Zhang J, Gao Y, Xue Q, Hu L, Xu T (2006) Grain size effect in corrosion behavior of electrodeposited nanocrystalline Ni coatings in alkaline solution. *Scr Mater* 55:657–660. <https://doi.org/10.1016/j.scriptamat.2006.04.009>
 49. Skale S, Doleček V, Slemnik M (2007) Substitution of the constant phase element by Warburg impedance for protective coatings. *Corros Sci* 49:1045–1055. <https://doi.org/10.1016/j.corsci.2006.06.027>
 50. Han L, Koide N, Chiba Y, Mitate T (2004) Modeling of an equivalent circuit for dye-sensitized solar cells. *Appl Phys Lett* 84:2433. <https://doi.org/10.1063/1.1690495>
 51. Yadav AP (2009) Electrochemical impedance response of Zn and galvanized steel corroding under marine atmospheric environments. *J Nepal Chem Soc* 23:33–42. <https://doi.org/10.3126/jncs.v23i0.2094>
 52. Galvan-Martinez R, Orozco-Cruz R, Carmona-Hernandez A, Mejia-Sanchez E, Morales-Cabrera MA, Contreras A (2019) Corrosion study of pipeline steel under stress at different cathodic potentials by EIS. *Metals* 9(12):1353
 53. Oliveira VMCA, Vazquez AM, Aguiar C, Robin A, Barboza MJR (2015) Protective effect of plasma-assisted PVD deposited coatings on Ti-6Al-4 V alloy in NaCl solutions. *Mater Des* 88:1334–1341. <https://doi.org/10.1016/j.matdes.2015.08.158>
 54. Eliaz N, Venkatakrishna K, Electroplating Hegde AC (2010) characterization of Zn–Ni, Zn–Co and Zn–Ni–Co alloys. *Surf Coat Tech* 205:1969–1978. <https://doi.org/10.1016/j.surfcoat.2010.08.077>
 55. Peng S, Xie SK, Lu JT, Zhang LC (2017) Surface characteristics and corrosion resistance of spangle on hot-dip galvanized coating. *J All Com* 728:1002–1008. <https://doi.org/10.1016/j.jallcom.2017.09.091>
 56. Daoud L, Belhamzaoui A, Amirat A (2017) Comparison between IEF model and numerical method based on the derivation method of Bridgman to evaluating fracture toughness in galvanized steel sheet. *Inter J Adv Manuf Technol* 92:569–581. <https://doi.org/10.1007/s00170-017-0097-4>
 57. Abou-Krishna MM (2012) Effect of pH and current density on the electrodeposition of Zn–Ni–Fe alloys from a sulfate bath. *J Coat Tech Res* 9:775–783. <https://doi.org/10.1007/s11998-012-9402-1>
 58. Lindström R, Svensson J-E, Johansson LG (2000) The atmospheric corrosion of Zinc in the presence of NaCl: the influence of carbon dioxide and temperature. *J Electrochem Soc* 147(5):1751–1757

Publisher's Note Springer Nature remains neutral with regard to jurisdictional claims in published maps and institutional affiliations.